



Original Articles

Identification of a novel ferroptosis-inducing micropeptide in bladder cancer



Weijian Li ^{a,b,1}, Ye Shen ^{c,1}, Chen Yang ^{a,b,1}, Fangdie Ye ^{a,b}, Yingchun Liang ^{a,b}, Zhang Cheng ^{a,b}, Yuxi Ou ^{a,b}, Wensun Chen ^{a,b}, Ziang Chen ^{a,b}, Lujia Zou ^{a,b}, Yufei Liu ^{a,b}, Yun Hu ^{a,b}, Xiang Yan ^{d,**}, Haowen Jiang ^{a,b,e,f,*}

^a Department of Urology, Huashan Hospital, Fudan University, Shanghai, China

^b Fudan Institute of Urology, Huashan Hospital, Fudan University, Shanghai, China

^c Department of Urology, Northern Jiangsu People's Hospital, Clinical Medical College of Yangzhou University, Yangzhou, China

^d Department of Urology, Pediatric Urolith Center, Children's Hospital, Zhejiang University School of Medicine, National Clinical Research Center for Child Health, China

^e National Clinical Research Center for Aging and Medicine, Fudan University, Shanghai, China

^f Department of Urology, Jing'an District Central Hospital, Fudan University, Shanghai, China

ARTICLE INFO

ABSTRACT

Keywords:

TRIM25
USP7
Ferroptosis
Cancer
Ubiquitination

Bladder cancer (BC) is a common malignancy in males, and currently lacks ideal therapeutic approaches. Exploring emerging therapeutic targets from the perspective of endogenous peptides to improve the prognosis of bladder cancer patients holds promise. In this study, we have identified CTSGDP-13, a novel endogenous peptide, which demonstrates potential anti-cancer effects in BC. Our findings reveal that CTSGDP-13 can promote ferroptosis in BC cells, both *in vitro* and *in vivo*, leading to the inhibition of BC progression. Furthermore, we have identified TRIM25 as a downstream regulatory target of CTSGDP-13. The expression of TRIM25 is significantly upregulated in BC, and its inhibition of ferroptosis promotes BC progression. Mechanistic studies have shown that CTSGDP-13 promotes the ubiquitination and subsequent degradation of TRIM25 by disrupting its interaction with the deubiquitinase USP7. Further investigations indicate that CTSGDP-13 promotes ferroptosis in BC by regulating the USP7/TRIM25/KEAP1 axis. The elucidation of the functional mechanisms of natural CTSGDP-13 and TRIM25 holds promise in providing valuable therapeutic targets for BC diagnosis and treatment.

1. Background

Bladder cancer (BC) has been confirmed as the 10th most common cancer worldwide, with around estimated 549,000 new cases and 200,000 deaths per year [1]. BC can fall into non-muscular invasive BC (NMIBC) or muscular invasive BC (MIBC), which is dependent on the degree of invasion [2,3]. NMIBC accounts for nearly 75 % of all BC types, whereas at least half of patients with NMIBC exhibit a high recurrence rate or progression to MIBC in 5 years [4]. The 5-year overall survival rate for MIBC patients reaches nearly 60%–70 %, suggesting the lack of effective diagnosis and treatment [5]. Accordingly, novel, especially natural, early diagnostic biomarkers and therapeutic targets should be urgently developed for BC [6].

Peptides with unique biological activities are formed by amino acids connected by peptide bonds. Endogenous peptides, produced by the body under physiological conditions, are primarily derived from the enzymatic hydrolysis of endogenous proteins or encoded by non-coding RNA [7]. Increasing studies have confirmed that endogenous peptides take on vital significance in the progression of cancer [8]. For instance, ALM201, a FKBPL-based peptide, has been reported to target angiogenesis and cancer stem cells in ovarian cancer [9]. Lise Nannan et al. reported that AG-9 and VG-6 peptides derived from tropoelastin could favor tumor progression in pancreatic ductal adenocarcinoma [10]. Furthermore, some peptide drugs have been developed to be the preferred therapeutic drugs for clinically advanced cancer patients [11]. Thus, endogenous peptides that are differently expressed in BC should

* Corresponding author. Department of Urology, Huashan Hospital, Fudan University; Fudan Institute of Urology, Huashan Hospital, Fudan University; Department of Urology, Jing'an District Central Hospital, Fudan University, Shanghai, China.

** Corresponding author.

E-mail addresses: yanxiang@zju.edu.cn (X. Yan), haowj_sh@fudan.edu.cn (H. Jiang).

¹ These authors contributed equally: Weijian Li, Ye Shen, Chen Yang.

be identified, which is promising to develop diagnostic and therapeutic targets.

In 2012, Scott J Dixon et al. found an iron-dependent form of non-apoptotic cell death and named it “ferroptosis” [12]. Ferroptosis, an emerging regulated cell death (RCD), is driven by iron dependence, lipid peroxidation, membrane damage, as well as cell lysis [13]. System XC⁻ refers to a transmembrane protein complex containing subunits SLC7A11 (i.e., xCT) and SLC3A2. Cystine is transported into cells through System XC⁻ and then reduced to cysteine, thus serving as a rate-limiting substrate for the synthesis of reduced glutathione (GSH) [14]. GSH has been confirmed as the most abundant reducing agent in mammal cells, and it is capable of helping glutathione peroxidase 4 (GPX4) neutralize phospholipid hydroperoxides (PLOOHs), i.e., a vital driving factor of ferroptosis [15]. Accordingly, SLC7A11 takes on critical significance in regulating ferroptosis [16]. The roles played by ferroptosis in multiple cancers have been reported recently [17]. Some research has confirmed the regulatory role of ferroptosis in BC, whereas the mechanism of ferroptosis in BC should be revealed in depth.

In this study, several endogenous peptides that were remarkably differentially expressed in BC were identified using mass spectrometry. To be specific, CTSGDP-13, a novel endogenous peptide derived from Cathepsin G, has aroused our attention for its significant anti-cancer effects in BC. As indicated by the result of this study, CTSGDP-13 exhibited the capability of facilitating ferroptosis of BC by regulating the USP7/TRIM25/KEAP1 axis. This study can provide potential early diagnostic markers and therapeutic targets for BC patients.

2. Materials and methods

2.1. Patients and tissue specimen collection

The collection of human tissue samples conformed to the Declaration of Helsinki and gained approval from the Board and Ethics Committee of Huashan Hospital, Fudan University (No. KY2011-009). Each patient provided written informed consent before tissue samples were collected. The respective patient signed an informed consent prior to the collection. Moreover, patients with a history of other cancers or who had undergone chemotherapy or radiotherapy before surgery were excluded. One BC tissue and one adjacent normal urothelial tissue were collected from the respective patient underwent radical cystectomy. The paraffin-embedded BC tissues (N = 38) and adjacent normal tissues (N = 38) were collected from BC patients. Three pairs of BC and adjacent normal tissues (stored in -80 °C) were selected for tandem mass tag (TMT) labeling and Liquid Chromatography-Mass Spectrometry/Mass Spectrometry (LC-MS/MS) analysis to identify differentially expressed endogenous peptides in BC. The patient clinical information from which these three tissue pairs were sourced is shown in Table S4. All collected samples was placed in cryovials and then stored in -80 °C after being rapidly frozen with liquid nitrogen.

2.2. Malondialdehyde (MDA) assay

MDA levels was detected following the previous description [18]. In brief, the relative levels of MDA in differently treated cell lysates were evaluated using the lipid peroxidation detection kit (MDA) (ab118970, Abcam) in accordance with the manufacturer’s instructions. MDA and thiobarbituric acid (TBA) react to produce MDA-TBA adducts in the sample, and the relative level of MDA can be detected by examining the absorbance of the MDA-TBA adducts using colorimetry.

2.3. Glutathione (GSH) assay

The detection of GSH levels was carried out according to the previous method [19]. Relative GSH concentrations in cells of the respective treatment group were determined using a glutathione detection kit (Beyotime, China) in accordance with the manufacturer’s

recommendations.

2.4. Immunohistochemistry (IHC)

IHC was performed as previously reported [20,21]. A total of 38 pairs of BC tissues were acquired for IHC. Table S3 lists the concentrations of antibodies applied in this study. The stained samples were identified under an Olympus microscope (Tokyo, Japan), and each IHC image was analyzed and then scored using ImageJ software (NIH, USA).

2.5. Cell culture

UMUC-3, T24, and 293T cells originated from the Type Culture Collection (Shanghai, China) at the Chinese Academy of Sciences. T24 and UMUC-3, 293T cells were cultured in high glucose Dulbecco’s modified Eagle’s medium (DMEM) (Gibco, USA) supplemented with 10 % fetal bovine serum (FBS), 100 units/mL penicillin, and 100 mg/mL streptomycin. The cells were cultured in a humidified environment (37 °C) supplemented with 5 % CO₂.

2.6. Synthesis of peptides

The 95 % purity of CTSGDP-13 and the scramble peptide were synthesized by the Scientific Peptide Biological Technology Co, Ltd. (Shanghai, China). After preliminary experiment and exploration, the concentration of CTGDP-13 and the scramble peptide used in cell experiments was 0.4 mg/mL in this study.

2.7. LC-MS/MS analysis

The sample to be analyzed for lysis was supplemented with a lysate containing 8 M urea and 100 mM Tris-Cl at pH 8.0. Subsequently, ultrafiltration was performed on the sample with an ultrafiltration tube that exhibited a pore size of 10 kD. After the sample was centrifuged (12,000 g, 15 min), the supernatant was extracted for desalting. The desalted peptide solution was concentrated and then stored at -20 °C, with the aim for mass spectrometry analysis. Mass spectrometry was performed based on a Thermo Q Exactive Plus LC/MS system. The samples were separated using a liquid phase UltiMate 3000 RSLCnano system. The peptide samples were dissolved and then bound to a C18 trapping column (3 μm, 120 Å, 100 μm × 20 mm). Next, the samples were separated with an analytical column (2 μm, 120 Å, 750 μm × 150 mm). An analytical gradient was developed using two mobile phases (mobile phase A: 3 % Dimethyl Sulfoxide (DMSO), 0.1 % formic acid, 97 % HO; mobile phase B: 3 % DMSO, 0.1 % formic acid, 97 % acetonitrile).

2.8. Colony formation assay

After being subjected to different treatments, cells in the respective group were seeded at a density of 100 cells per well into 12-well plates. Next, the cells were allowed to grow in a medium supplemented with 10 % FBS for approximately 7–10 days. Following the above-mentioned incubation period, the medium was removed from the respective well, and the cells were washed with Phosphate-Buffered Saline (PBS), fixed with 4 % paraformaldehyde, and then stained with 0.1 % crystal violet. Lastly, the number of cell colonies in the respective well was imaged and then analyzed.

2.9. Cell viability assay

Cell viability was evaluated using the Cell Counting Kit-8 (CCK-8). The cells from the different treated groups were seeded into 96-well plates at a density of 1000 cells per well, with five replicate wells in the respective group. After the samples were incubated for the indicated time points, the CCK-8 reagent (MedChemExpress, USA) was introduced in accordance with the manufacturer’s instructions. The absorbance was

examined at 450 nm with a microplate reader.

2.10. EdU assay

The EdU detection kit (Ribobio, China) was employed in accordance with the manufacturer's instructions to detect DNA synthesis and cell proliferation. In brief, BC cells from the different groups were grown on slides and labeled with the EdU working solution. After incubation, fixation, and washing, DNA synthesis and cell proliferation were observed using a fluorescence microscope (Nikon, Japan).

2.11. Transwell assays

For the migration assay, 5×10^4 BC cells from different treatment groups were placed into the upper chamber (Corning, USA) supplemented with 200 μ l of serum-free medium. Next, the upper chamber was placed into a well containing 600 μ l of medium supplemented with 20 % FBS. After incubation for 24 h, the upper chamber was removed, and the cells were fixed with 4 % paraformaldehyde at ambient temperature for 20 min, stained with 0.1 % crystal violet (Sigma, USA), and imaged under a microscope (Nikon, Japan). The protocol for the invasion assay is similar to the migration assay, except that Matrigel (BD Biosciences, USA) needs to be introduced to the upper chamber in advance and solidified (37 °C, overnight). In addition, the cells were incubated for 48 h.

2.12. Wound healing assay

To perform the wound healing assay, BC cells were seeded in 6-well plates and allowed to grow to approximately 90 % confluence in medium supplemented with 10 % FBS. A wound was made on the bottom cell-covered surface of the respective well using a 200 μ l pipette tip. Images of each wound were acquired at 0 h and 24 h using an inverted microscope (Nikon, Japan). The wound healing rate was analyzed using ImageJ software (NIH, USA).

2.13. RNA extraction and quantitative real-time PCR (qRT-PCR)

Total RNA was extracted with Trizol reagent (Invitrogen, USA), and reverse transcription was performed using the PrimeScript™ RT Reagent Kit (TaKaRa, Japan) in accordance with the manufacturer's instructions. Subsequently, the cDNA was subjected to qRT-PCR using an ABI 7900HT sequence detector (Thermo Fisher Scientific, USA). GAPDH served as an internal reference for mRNA detection. The respective sample was repeated three times, and the results were analyzed based on the $\Delta\Delta CT$ method. The primer sequences used are shown in Table S3.

2.14. Lentivirus preparation and infection

The lentiviruses employed in this study originated from Ribobio (Guangzhou, China). UMUC3 and T24 cells were infected with the lentivirus and then selected with 10 μ M puromycin for one week to develop stably transfected cell lines. Table S3 lists the detailed sequence information.

2.15. Reactive oxygen species (ROS) level

The total cellular levels of ROS were detected using a reactive oxygen species detection kit (Thermo Fisher Scientific, USA) following the manufacturer's instructions. DCFH-DA was used to detect the levels of total ROS in the respective group of cells. The results were observed using confocal fluorescence microscopy and analyzed by flow cytometry.

2.16. Lipid peroxidation assay

Analysis of relative lipid peroxidation levels in cells was performed

using C11-BODIPY dye in accordance with the manufacturer's suggestions (Thermo Fisher Scientific, USA). Specifically, cells were treated with C11-BODIPY probe (5 μ m, 30 min), collected and washed twice with PBS, and resuspended in 500 μ l PBS. The levels of lipid peroxidation were analyzed by flow cytometry (FACSCanto™ II, BD Biosciences).

2.17. Fe^{2+} detection assay

According to the manufacturer's instructions, intracellular Fe^{2+} levels were measured using an iron assay kit (MesGenBiotech, USA). In brief, optical density was determined at 520 nm using a microplate reader (Thermo Fisher Scientific, USA), and the relative concentration of Fe^{2+} was calculated accordingly.

2.18. Immunofluorescence (IF)

FITC-labeled CTSGDP-13 was introduced into T24 and UMUC3 cells cultured on coverslips. After fixing the cells with 4 % paraformaldehyde, they were blocked with an anti-TRIM25 antibody and then labeled with fluorescence-coupled FITC. Subsequently, the coverslips were stained with 4',6-diamidino-2-phenylindole (DAPI, Invitrogen) to highlight the nuclei, and the cells were identified under a confocal fluorescent microscope (Olympus, Japan).

2.19. Immunoprecipitation (IP)

The whole cell lysates collected from the respective group were centrifuged for 30 min (4 °C, 12000 rpm). Protein A/G magnetic beads (Thermo Scientific Fisher, USA) were used for the preclearing process to eliminate non-specific binding between proteins and magnetic beads in the whole cell lysates. The whole-cell lysates were assigned to three groups (i.e., Input group, IgG group, and IP group). The respective antibody and cell lysates were incubated separately overnight at 4 °C. The antibody and cell lysates were incubated separately overnight at 4 °C. Subsequently, protein A/G magnetic beads were incubated with antibody-protein complexes overnight at 4 °C. The magnetic beads were extracted with a magnetic stand, washed with a washing buffer largely supplemented with 0.1 % TritonX-100, 50 mM Tris-HCl, and 5 mM EDTA, and then washed with pre-cooled PBS. The elution of protein/biotin-peptide-protein complexes was primarily performed using glycine. The eluted product was analyzed through Western Blotting analysis.

2.20. Transmission electron microscopy (TEM)

Cells from different groups were collected and washed repeatedly with PBS (1×10^7 for the respective group). After centrifugation, cells were mixed with agarose and fixed with 1 % OsO₄ (Ted Pella Inc). Then, the samples were dehydrated several times at ambient temperature using different concentrations of ethanol. The resin-infiltrated and embedded samples were polymerized in a 65 °C oven and sliced into thin slices on an ultramicrotome (Leica UC7, Germany). Lastly, mitochondrial images were obtained using a transmission electron microscope (HT7800/HT7700, HITACHI, Japan).

2.21. Animal study

Four-week-old female BALB/c nude mice originated from SLARC (Shanghai, China) and adaptively fed for one week under specific-pathogen-free (SPF) conditions. In the subcutaneous xenograft tumor model, 72 nude mice were randomly assigned to groups of six each. BC cells stably expressed fluorescein (T24: 5×10^6 /mouse, UMUC3: 2×10^6 /mouse). The long diameter (L) and wide diameter (W) of the tumor were examined with a vernier caliper every seven days. The tumor volume (V) was estimated using formula $V = (W^2 \times L)/2$. CTSGDP-13 or

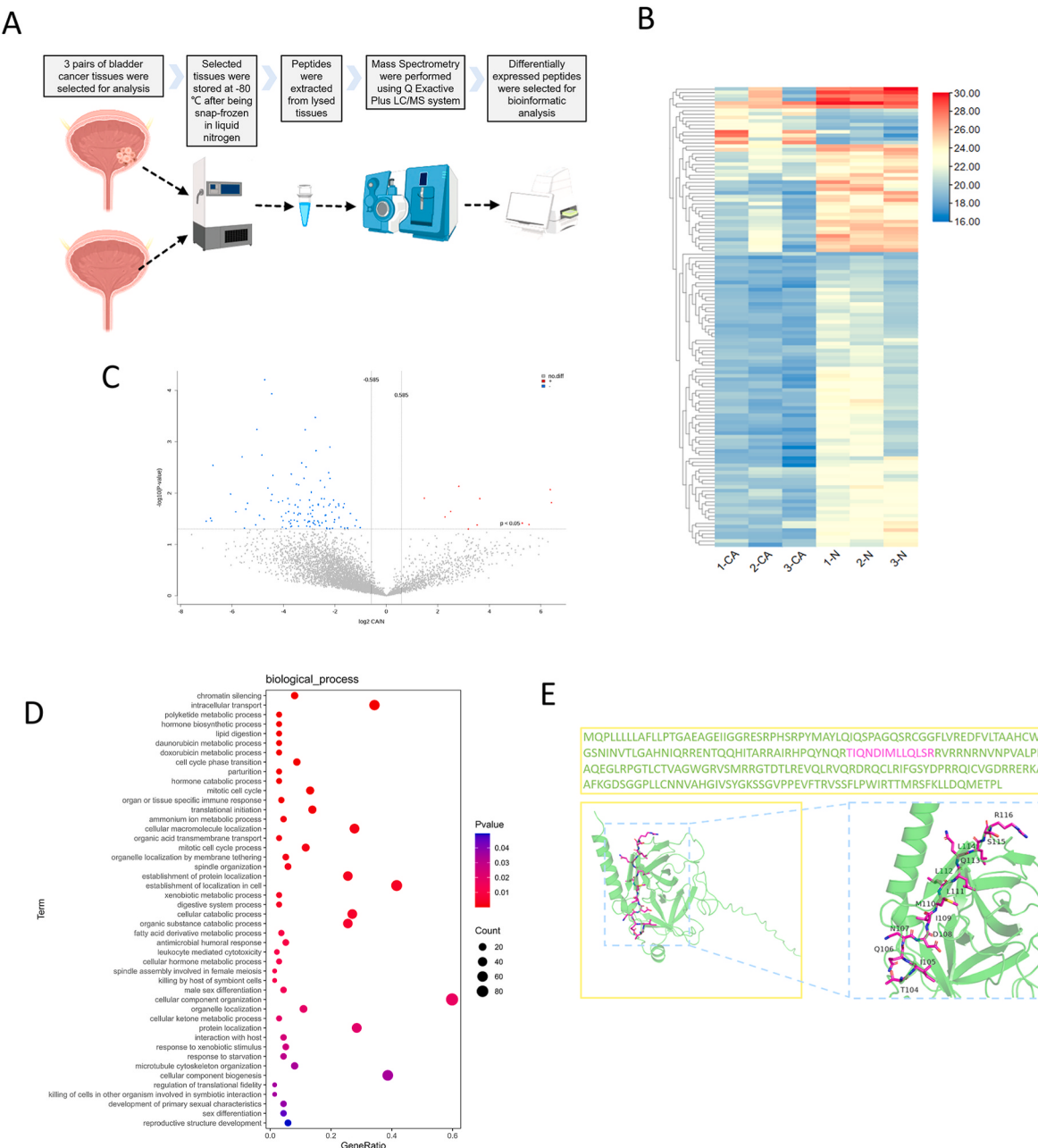


Fig. 1. Identification of CTSGDP-13 in bladder cancer. (A) Flowchart illustrating the collection of BC tissues and subsequent LC-MS/MS analysis. (B) Heatmap displaying the differential expression of endogenous peptides in BC. (C) Volcano plot depicting the differential expression of peptides in BC. (D) Representative GO terms of the prerequisite protein of dysregulated peptides (biological process). (E) Schematic diagram outlining the structure of CTSGDP-13. *P < 0.05, **P < 0.01, ***P < 0.001.

Scr (10 mg/kg) peptide was injected intraperitoneally 8, 12, 16, 20 days after tumor cells injection. 28 days after tumor cells injection, fluorescein was injected intraperitoneally, and the tumor growth was analyzed based on In Vivo Imaging System. Mice were sacrificed six weeks after cell injection, and the tumors were removed and then weighed. In the tail-vein injection metastasis model, 36 nude mice were randomly assigned to groups of six each. The BC cells (1×10^5) stably expressing fluorescein in different groups (Vector, TRIM25) were intravenously injected into the mice. CTSGDP-13 or Scr (10 mg/kg) was injected intraperitoneally 8, 12, 16, 20 days after tumor cell injection. 28 and 40 days later, fluorescein was injected intraperitoneally, and the lung metastasis of the tumor was studied using In Vivo Imaging System respectively. Mice were sacrificed 42 days after cell injection, and lung tissues were removed (Fig. 8A).

2.22. Bioinformatics

The structure of CTSGDP-13 peptide was drawn using ChemBioDraw Ultra 14.0, and the structure was imported into ChemBio3D Ultra 14.0 for energy minimization. The structural information of TRIM25 was downloaded from the PDB database. The peptide and protein structures were uploaded to HPEPDOCK for docking, and the interaction mode analysis of the docking results was conducted based on PyMOL2.3.0. The single-cell data used in the analysis was obtained from GSE135337. The Seurat package was the R package applied for single-cell data processing. The FindNeighbors and FindClusters functions (dim = 20, resolution = 0.8) were used for clustering analysis. Dimensionality reduction was performed using the RunUMAP function. The Cancer Genome Atlas (TCGA) program patients were divided into high-expression group and

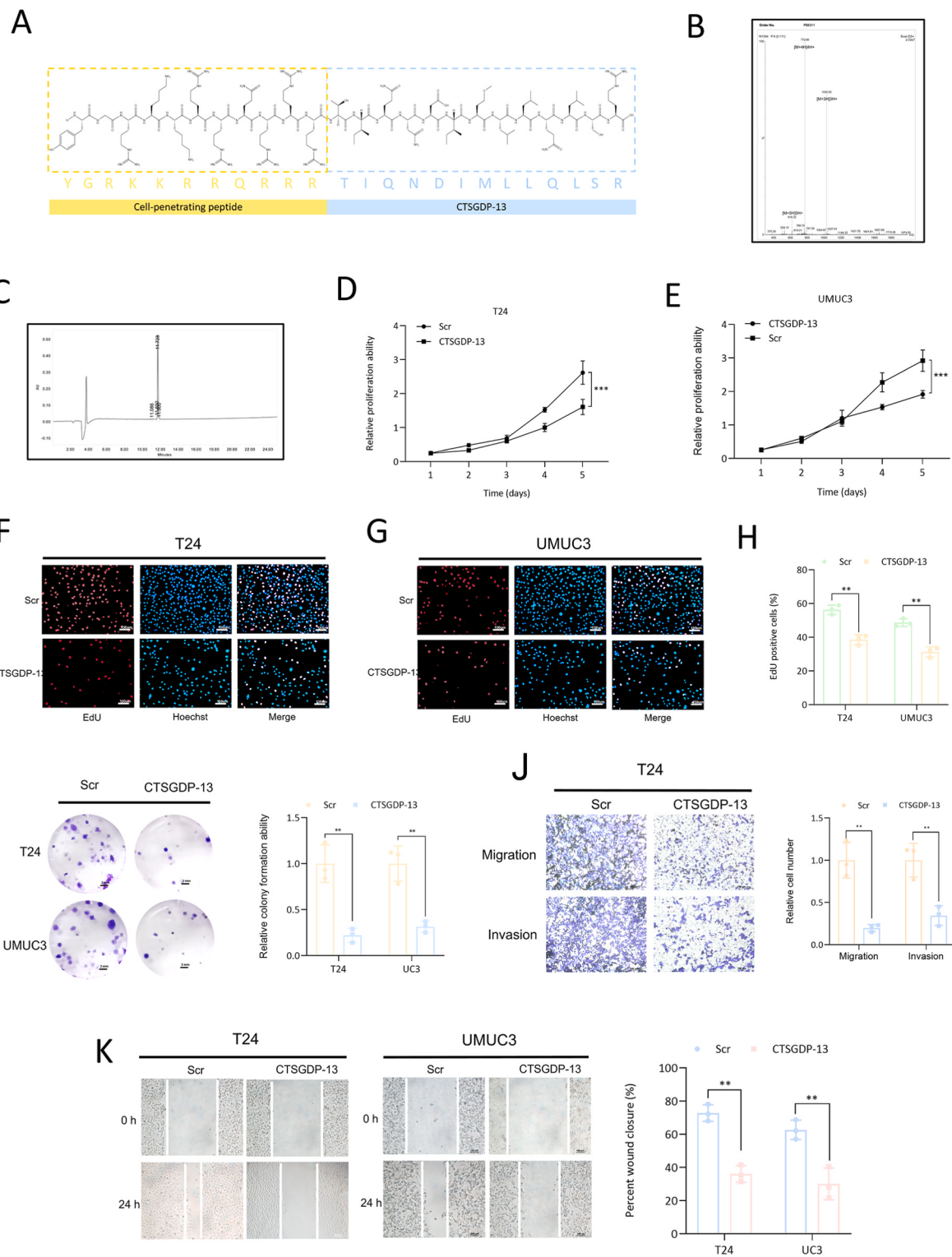


Fig. 2. CTSGDP-13 inhibits the proliferation, migration and invasion of BC cells. (Peptide concentration: 0.4 mg/mL) (A) Sequence information of CTSGDP-13 carrying cell-penetrating peptide. (B) Mass spectrum of synthesized CTSGDP-13. (C) Liquid chromatogram of synthesized CTSGDP-13. The proliferation ability of T24 cells (D) and UMUC3 cells (E) was assessed using the CCK-8 assay after treatment with Scr or CTSGDP-13. The proliferation ability of T24(F) and UMUC3(G) from different group was detected using EDU assay. Scale bar: 150um. (H) Quantitative analysis of EDU assay results. (I) The proliferation ability of BC cells was evaluated using the colony formation assay after treatment with Scr or CTSGDP-13. Scale bar: 2 mm. (J) Transwell assay revealed the migration and invasion abilities of T24 cells treated with Scr or CTSGDP-13. Scale bar: 100um. (K) Wound healing assay showing the migration ability of BC cells treated with Scr or CTSGDP-13. Scale bar: 100um. *P < 0.05, **P < 0.01, ***P < 0.001.

low-expression group based on TRIM25 mRNA expression. The R package employed for difference analysis was limma, with false discovery rate (FDR) < 0.05 and $|\log_2[\text{fold change (FC)}]| > 2$ adopted as the criteria for differences. Heatmaps for Kyoto Encyclopedia of Genes and Genomes (KEGG) pathway analysis were drawn using the pheatmap package. The R package used for the Kaplan-Meier survival analysis was Survminer, with Stage I and patients with unclear stages being screened out during survival analysis. The flow chart in Fig. 1A was drawn by Medpeer, and the flow charts in Fig. 4A and 8A were generated using Figdraw. Western blot analysis.

Western blot analysis was performed using the previously reported method [22–24]. In brief, the cells from different groups were lysed using RIPA buffer supplemented with protease inhibitors (Beyotime, China) and phosphatase inhibitors (Bimake, USA) in accordance with the manufacturer's instructions (Beyotime, China), with the aim of extracting total protein. The protein concentration in the extracted lysate was examined with the BCA kit (Thermo, USA), and 1/4 volume of the lysate was mixed with 5 × loading buffer and heated (95 °C, 10 min) before storing at –80 °C. The extracted proteins were separated through electrophoresis on 8–12 % Sodium Dodecyl Sulfate Polyacrylamide Gel Electrophoresis (SDS-PAGE) gels and then transferred to polyvinylidene difluoride (PVDF) membranes (Millipore, USA). After blocking with non-fat milk for 1 h, the PVDF membranes were incubated with the indicated antibodies (4 °C, overnight). Subsequently, the membranes were incubated with a peroxidase (HRP)-conjugated secondary antibody (1 h, ambient temperature). After washing, enhanced chemiluminescence (ECL) solution (CLiNX, Shanghai, China) was introduced to the membrane, and the bands on the PVDF membrane were detected using an ECL imaging system (CLiNX, Shanghai). Image J software (NIH, USA) was used for quantitative analysis. Table S3 lists all antibody product information.

2.23. Biotin pull-down assay and silver staining

Biotin pull down assay and silver staining were performed in accordance with existing research [25]. Biotinylated scramble peptide and biotinylated CTSGDP-13 originated from Scientific Peptide Biological Technology Co, Ltd. (Shanghai, China). 2 µg of biotinylated CTSGDP-13 was incubated with Dynabeads™ M – 280 Streptavidin Beads (Invitrogen) (4 °C, overnight). Whole-cell lysates were centrifuged for 30 min (4 °C, 12,000 rpm) and then precleared with Dynabeads™ M – 280 Streptavidin Beads to eliminate non-specific binding. Next, the pre-cleared lysate was incubated with the magnetic beads-biotinylated peptide complex (4 °C, overnight). The magnetic beads were separated from the solution with a magnetic stand, cleaned with a buffer supplemented with 0.1 % TritonX-100, 50 mM Tris-HCl, and 5 mM EDTA, and then washed using pre-cooled PBS. Afterward, the biotin-peptide complex was eluted with glycine. The eluted solution was separated through electrophoresis on a 10 % SDS-PAGE gel and then silver stained in accordance with the manufacturer's instructions (Beyotime Biotechnology, Shanghai). In brief, the gel was immersed in 100 mL of fixative solution and shaken at ambient temperature for 20 min at 60–70 rpm. Then, it was washed with 30 % ethanol and Milli-Q pure water on a shaker for 10 min at 60–70 rpm. Subsequently, the gel was sensitized with 100 mL of silver staining sensitizing solution for 2 min at 60–70 rpm and washed twice for 1 min at 60–70 rpm. The gel was then silver stained with 100 mL of silver solution (1 ×) for 10 min at 60–70 rpm. After washing, the silver-stained gel was developed with silver staining solution and color development was stopped after 10 min. The gel was photographed, and then analyzed through mass spectrometry.

2.24. Statistical analysis

Statistical differences among different experimental groups were evaluated using Microsoft Office Excel and GraphPad Prism. The data

are expressed as mean ± standard deviation (SD) of three independent experiments. P ≤ 0.05 indicated a difference that achieved statistical significance (**<0.05; **P < 0.01; ***P < 0.001). The respective group of experiments was independently repeated three times.

3. Results

3.1. Identification of CTSGDP-13 in BC

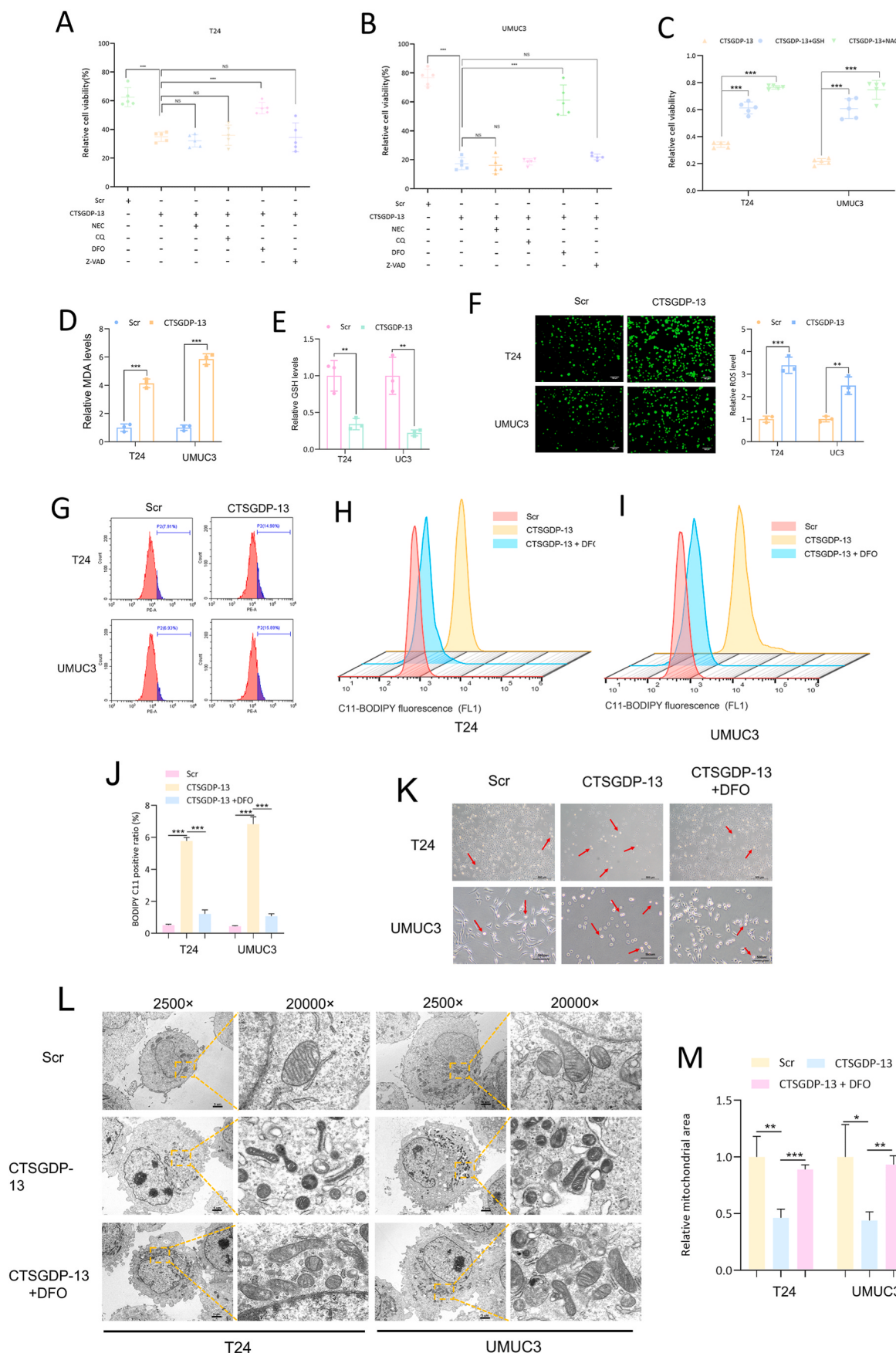
As depicted in Fig. 1A, three pairs of BC tissue samples were randomly selected from the collected 38 pairs of BC tissue for LC-MS/MS analysis. Bioinformatics analysis was performed on peptides differentially expressed in BC, and a total of 128 endogenous peptides were identified as being differentially expressed ($|\log_2[\text{fold change (FC)}]| > 2$). To be specific, 11 peptides were up-regulated, and 117 peptides were down-regulated (Fig. 1B and C). Representative peptides differentially expressed in BC are listed in Table S1. Based on the precursor proteins of the above-mentioned differentially expressed peptides, we performed Gene Ontology (GO) analysis and KEGG pathway analyses. GO analysis revealed that the above-described peptides may participate in GO terms that regulate cancer cells (e.g., “chromatin silencing” and “translational initiation”) (Fig. S1A-B, Fig. 1D). As revealed by KEGG pathway analysis, the dysregulated peptides may play a certain role in multiple pathways closely related to cancer (e.g., “Necroptosis,” “Apoptosis,” “viral carcinogenesis,” and “chemical carcinogenesis”) (Fig. S1C). Domain has been confirmed to take on critical significance in protein function, and the position of the above-described differentially expressed peptides in the precursor protein was analyzed. Table S2 presented the differentially expressed peptides that located in the domains of the precursor proteins. Based on the above analysis, TIQNDIMLLQLSR, located in the functional domain of the precursor protein Cathepsin G and notably down-regulated in BC, suggested its potential anticancer function, which aroused the attention of our team. Structural analysis revealed that TIQNDIMLLQLSR refers to a 13-peptide derived from amino acids 104–116 of Cathepsin G protein, termed Cathepsin G Derived Peptide-13 (CTSGDP-13) (Fig. 1E).

3.2. CTSGDP-13 inhibits the proliferation, migration and invasion of BC

To investigate the potential anticancer effects of CTSGDP-13, we synthesized CTSGDP-13 and its scrambled (Scr) peptide fused with a cell-penetrating peptide (Fig. 2A). The accuracy of the synthesized peptide sequences was confirmed through mass spectrometry and liquid chromatograph (Fig. 2B and C). CCK-8 assay revealed that, compared with Scr, CTSGDP-13 remarkably inhibited the proliferation of BC cells (Fig. 2D and E). Similarly, the EDU assay demonstrated that CTSGDP-13 could notably suppress the proliferation of BC cells in comparison to the scramble peptide (Fig. 2F–H). Additionally, the colony formation assay revealed that BC cells in the CTSGDP-13 group exhibited remarkably lower proliferation ability than those in the Scr group (Fig. 2I). Transwell assay showed that the migration and invasion abilities of BC cells in the CTSGDP-13 group were notably reduced in comparison to the Scr group (Fig. 2J, S2A). The wound healing assay also demonstrated that CTSGDP-13 could remarkably inhibit the migration ability of BC cells (Fig. 2K). As revealed by the result of Western Blotting analysis, the markers correlated with metastasis were notably changed in the CTSGDP-13 group, suggesting a weakened migration and invasion capacity in BC cells (Fig. S2B).

3.3. CTSGDP-13 promotes ferroptosis in BC cells

The ways of cell death mainly include apoptosis, autophagy, necroptosis, ferroptosis, etc. To determine which death way CTSGDP-13 induces BC cell death, we used inhibitors of different cell death pathways in combination with CTSGDP-13. Our results indicated that co-treatment with necrostatin-1 (a necroptosis inhibitor), Chloroquine



(caption on next page)

Fig. 3. CTSGDP-13 promotes ferroptosis in BC cells. (Peptide concentration: 0.4 mg/mL) The viability of T24 (A) and UMUC3 (B) cells treated with Scr, CTSGDP-13, NEC, CQ, DFO, and Z-VAD was assessed using the CCK-8 assay. (C) Viability of BC cells in CTSGDP-13, CTSGDP-13 + GSH, CTSGDP-13 + NAC groups were determined by CCK-8 assay. (D) MDA levels in BC cells treated with Scr or CTSGDP-13 were measured. (E) GSH levels in BC cells treated with Scr or CTSGDP-13 were measured. (F) ROS levels in BC cells after treated with Scr or CTSGDP-13 were detected by confocal fluorescence microscopy. Scale bar: 100μm. (G) Flow cytometry was used to determine ROS levels in BC cells after treated with Scr or CTSGDP-13. Lipid peroxidation levels in T24 (H) and UMUC3 (I) cells were detected using the C11-BODIPY probe. (J) Quantitative analysis of lipid peroxidation levels detected by C11-BODIPY probe was performed. (K) Morphological changes of BC cells after treatment with Scr, CTSGDP-13 or DFO were observed by microscopy. (The red arrows indicate BC cells in which ferroptosis occurs) Scale bar: 500μm. (L) Morphological changes of BC cell mitochondria after treatment with Scr, CTSGDP-13 or DFO were observed by TEM. Scale bar: 5μm. (M) Quantitative analysis of the mitochondrial area of BC cells observed in TEM was performed. *P < 0.05, **P < 0.01, ***P < 0.001.

(CQ, an autophagy inhibitor), and Z-VAD-FMK (a pan-caspase inhibitor) did not notably improve cell viability. However, when Desferrioxamine (DFO, a ferroptosis inhibitor) was used in conjunction with CTSGDP-13, we observed a significant improvement in cell viability, suggesting that CTSGDP-13 may induce ferroptosis in BC cells (Fig. 3A and B). Since iron-dependent lipid peroxidation is a crucial component of ferroptosis, we treated cells with the lipid peroxidation inhibitors glutathione (GSH) and N-acetylcysteine (NAC) in combination with CTSGDP-13 and found that cell viability inhibited by CTSGDP-13 was remarkably improved (Fig. 3C). Meanwhile, we detected the levels of lipid peroxidation markers MDA and GSH in BC cells, and found that CTSGDP-13 can notably increase the level of MDA and reduce the level of GSH in BC cells, indicating that CTSGDP-13 can promote lipid peroxidation in BC cells (Fig. 3D and E). In addition, we found that the total ROS level of BC cells in the CTSGDP-13 group was remarkably elevated relative to the Scr group (Fig. 3F and G). Using the C11-BODIPY probe, we detected an increase in the lipid peroxidation level in BC cells treated with CTSGDP-13, and this effect was notably rescued by DFO (Fig. 3H–J). We found that the cell death was remarkably increased after treated with CTSGDP-13, while DFO could inhibit such death of BC cells (Fig. 3K). Furthermore, using TEM, we found that BC cells in the CTSGDP-13 group had notably smaller mitochondria and increased membrane density compared with the Scr group, and DFO could remarkably rescue this change (Fig. 3L–M). In addition, we found that CTSGDP-13 can significantly increase levels of Fe²⁺ and ferroptosis markers TfR1 and ACSL4 in BC cells, and this effect can be restored by DFO (Figs. S2C–D). Our findings suggest that CTSGDP-13 functions as a tumor suppressor in BC by promoting ferroptosis in BC cells.

3.4. CTSGDP-13 promotes the degradation of TRIM25 by binding to the “coiled-coil” domain

Biotin pull-down assay was performed to investigate the molecular mechanism of CTSGDP-13 regulating BC (Fig. 4A). Biotin-labeled CTSGDP-13 and Scr were synthesized (Figs. S3A–B), and proteins that potentially interact with CTSGDP-13 were isolated on SDS-PAGE gel and then analyzed through silver staining (Fig. 4B). To be specific, a significant band around 70 KDa aroused the attention of our group and was identified as TRIM25 protein using mass spectrometry analysis (Fig. 4C). The molecular docking software suggested that the binding energy between TIQNDIMLLQLSR (CTSGDP-13) and TRIM25 was -173.497 kcal/mol, suggesting a high binding capacity between them (Fig. 4D). An IP assay was performed to clarify whether CTSGDP-13 interacts with TRIM25. The IP assay indicated that TRIM25 was interacted with CTSGDP-13 peptide (Fig. 4E). Besides, the result of IF assay revealed the co-localization of CTSGDP-13 and TRIM25 in BC cells (Fig. 4F). Western Blotting analysis found that CTSGDP-13 could reduce TRIM25 protein level in a dose-dependent manner (Fig. 4G). Interestingly, PCR analysis found that CTSGDP-13 did not affect the mRNA level of TRIM25 (Fig. S3C), suggesting that CTSGDP-13 regulates the expression of TRIM25 at the post-transcriptional level. Cycloheximide (CHX) were used to inhibit protein synthesis and Western Blotting analysis found that CTSGDP-13 facilitated the degradation of TRIM25. Meanwhile, MG132 (proteasome inhibitor) but not CQ (lysosome inhibitor) could notably inhibit the effect of CTSGDP-13 on TRIM25 (Fig. 4H), suggesting that CTSGDP-13 may affect its level by regulating the ubiquitination of

TRIM25. Western Blotting analysis revealed that ubiquitinated TRIM25 was increased in T24 cells and UMUC3 cells (Fig. 4I). TRIM25 mainly includes RING, coiled-coil (CC) and PRY/SPRY (PS) domains which are the basis of TRIM25 protein function. To study the specific binding site of CTSGDP-13 on TRIM25, we constructed four Flag-labeled plasmids containing different fragments of TRIM25 (Fig. 4J, S3D) for IP assay. IP assay revealed that CTSGDP-13 can bind to the CC domain of TRIM25 (Fig. 4K). The above-mentioned results suggest that CTSGDP-13 binds to the CC domain of TRIM25 to promote its ubiquitination.

3.5. CTSGDP-13 and deubiquitinase USP7 competitively bind to TRIM25

The mode through which the regulation of TRIM25 ubiquitination is mediated by CTSGDP-13 has incited our interest. Proteins interacting with TRIM25 have been identified via immunoprecipitation coupled with mass spectrometry analysis, with particular attention drawn to USP7 (Fig. 4L). USP7 serves as a deubiquitinating enzyme responsible for governing the ubiquitination process of substrate proteins. The interaction between USP7 and TRIM25 has been confirmed through our co-immunoprecipitation experiments (Fig. 4M). Furthermore, it has been observed that the promotion of TRIM25 ubiquitination induced by CTSGDP-13 is effectively counteracted by the significant overexpression of USP7 (Fig. 4N). Nevertheless, protein expression levels of USP7 have been determined to remain unaffected by CTSGDP-13 as demonstrated by Western blot assays (Fig. 4O). As such, we postulate that the functional impact of CTSGDP-13 stems from its disruption of the reciprocal interplay between USP7 and TRIM25, rather than its direct modulation of USP7 expression. The co-immunoprecipitation results imply that the interaction between USP7 and TRIM25 is notably diminished by CTSGDP-13 (Fig. 4P). These findings collectively indicate that CTSGDP-13 attenuates the stabilizing effect of deubiquitinating enzyme USP7 on TRIM25 by competitively disrupting their interaction, thereby promoting the ubiquitination degradation of TRIM25.

3.6. TRIM25 is upregulated in BC, and its silence promotes ferroptosis in BC

The role of TRIM25 in BC is still unclear. Bioinformatics analysis found that TRIM25 mRNA level was remarkably higher in BC than in normal group (Fig. 5A). However, the mRNA level of TRIM25 did not increase with the increase of BC stage (Fig. S4A). We further analyzed the expression of TRIM25 in BC at the single-cell level. Among eight samples (7 tumor tissues and 1 normal tissue), 10 cell clusters (e.g., epithelial cells, fibroblast cells, and B cells) were identified (Fig. 5B). TRIM25 expression was largely concentrated in epithelial cell, suggesting that TRIM25 may play a certain role in uroepithelial carcinoma (Figs. S4B–C). Meanwhile, Principal Component Analysis (PCA) was performed to explore the differences in metabolic status between the low and high expression subgroups of TRIM25. As indicated by PCA results, the contribution of Dim1 and Dim2 to the total variance took up 11.7 % and 30.7 %, respectively, in the TCGA dataset (Fig. 5C). In KEGG pathway analysis, heatmaps showed that TRIM25 was closely related to the “JAK-STAT”, “MAPK”, especially “Bladder cancer” signaling pathways, indicating that TRIM25 may play a potential regulatory role in BC (Fig. 5D). Furthermore, Kaplan-Meier analysis showed the progression free interval (PFI) of patients with higher expression of TRIM25 was

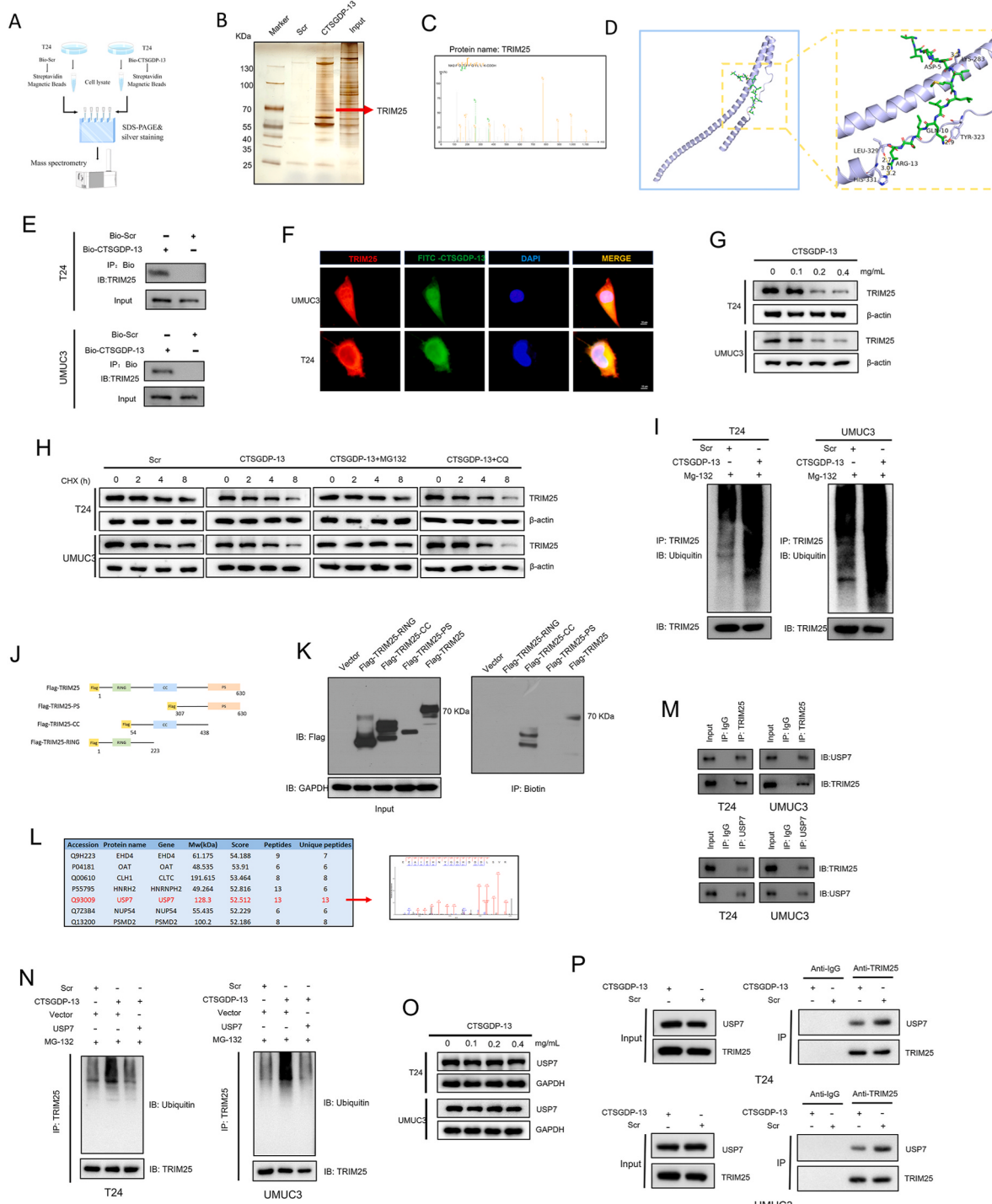


Fig. 4. Interaction of CTSGDP-13 with TRIM25. (A) Flowchart illustrating biotin pull-down. (B) Silver staining of the isolated biotin pull-down product separated on a 10 % SDS-PAGE gel. (C) Mass spectrum of TRIM25. (D) Molecular docking predictions of CTSGDP-13 and TRIM25. (E) IP assay confirmed the interaction between CTSGDP-13 and TRIM25 in BC cells. (F) IF assay confirmed the co-localization of CTSGDP-13 and TRIM25 in BC cells. Scale bar: 10um. (G) Western Blot analysis showed the protein levels of TRIM25 after treatment with different concentrations of CTSGDP-13 for 24 h. (H) Western blot analysis showed the protein level of TRIM25 in different groups after adding MG132. (I) Western blot analysis revealing the level of TRIM25 ubiquitination in BC cells after treatment with CTSGDP-13. (J) The structure of flag labeled plasmids containing different TRIM25 fragments. (K) IP assay revealed the interaction between the flag-labeled plasmid containing the coiled-coil domain and CTSGDP-13. (L) Mass spectrum of usp7 protein. (M) Co-IP assay revealed the interaction between TRIM25 and USP7. (N) Western blot analysis revealed the level of TRIM25 ubiquitination in BC cells after different treatment. (O) Western blot analysis revealed the level of USP7. (P) Co-IP assay revealed the interaction between TRIM25 and USP7 with or without CTSGDP-13. *P < 0.05, **P < 0.01, ***P < 0.001.

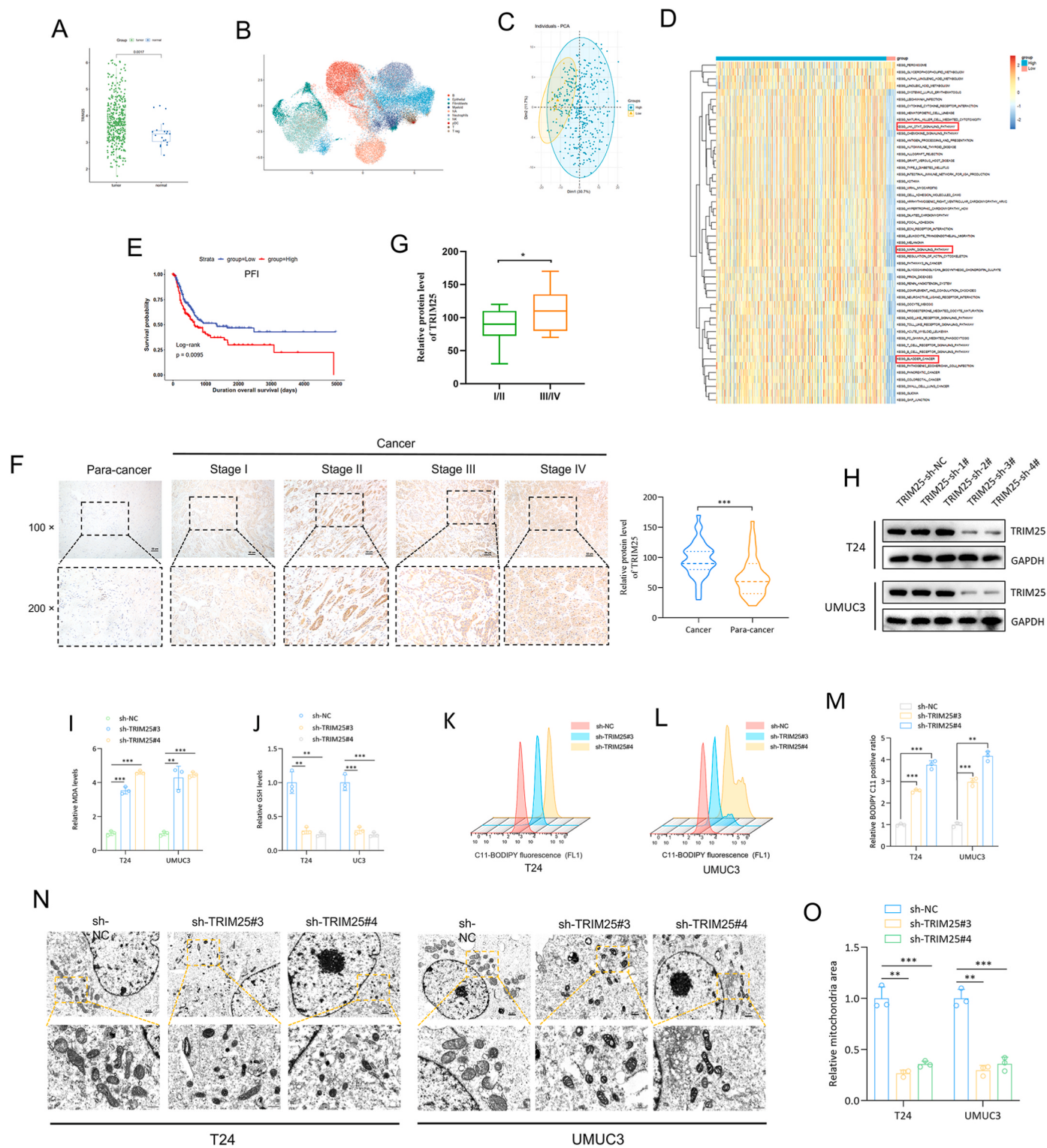


Fig. 5. TRIM25 up-regulated in BC and promoted ferroptosis in BC. (A) TRIM25 mRNA levels in BC tissues and normal tissues in TCGA. (B) T-SNE plot revealing the distribution of TRIM25 in different cell clusters. (C) PCA revealed the differences in metabolic status between the low and high expression subgroups of TRIM25. (D) Heatmaps revealed the KEGG pathway associated with TRIM25. (E) Kaplan-Meier analysis revealed that BC patients with high TRIM25 expression had a shorter PFI compared to those with low expression. (F) Immunohistochemical (IHC) analysis of 38 pairs of BC tissues demonstrated higher levels of TRIM25 protein in the BC group compared to the normal control group. Scale bar: 50um. (G) IHC analysis revealed the expression of TRIM25 in I/II and III/IV stage of BC. (H) Western blot analysis revealed TRIM25 protein levels after treatment of different shRNAs of TRIM25. (I) TRIM25 silencing was found to increase MDA levels. (J) TRIM25 silencing was found to decrease GSH levels. Lipid peroxidation levels in T24 cells (K) and UMUC3 cells (L) before and after TRIM25 silencing detected by C11-BODIPY probe. (M) Quantification of lipid peroxidation levels in BC cells. (N) Morphological changes of mitochondria in BC cells before and after TRIM25 silencing were observed by TEM. Scale bar: 5um. (O) Quantification of the mitochondrial area of BC cells. *P < 0.05, **P < 0.01, ***P < 0.001.

Table 1

Correlations between TRIM25 expression levels and the clinicopathological characteristics of BC patients.

Characteristics	Number of case (%)	TRIM25 expression		P value
		Low (%)	High (%)	
Total	38	19	19	
Gender				0.150
Male	33 (86.8)	18	15	
Female	5(13.2)	1	4	
Grade				0.034*
Low	4(10.5)	4	0	
High	34(89.5)	15	19	
Age (years)				0.305
< 70	25(65.8)	14	11	
≥70	13(34.2)	5	8	
Tumor size (cm)				0.009**
< 3	20 (52.6)	14	6	
≥3	18 (47.4)	5	13	
T stage				0.005**
T1-T2	26(68.4)	17	9	
T3-T4	12(31.6)	2	10	
N stage				0.016*
N0	30(78.9)	18	12	
N1	8(21.1)	1	7	
Muscle invasion				0.017*
Yes	25(65.8)	9	16	
No	13(34.2)	10	3	

*P < 0.05 is considered to be significant.

notably lower than those of the lower expression group (Fig. 5E). In addition, IHC staining of 38 pairs of BC tissue specimens from our cohort indicated that the expression level of TRIM25 was remarkably increased in BC (Fig. 5F). Moreover, the protein level of TRIM25 in III/IV stage is significantly higher than I/II stage BC (Fig. 5G). Furthermore, the Kaplan-Meier survival analysis conducted on our cohort (N = 38) revealed that patients with high TRIM25 expression exhibited notably poorer prognosis in comparison to those with low TRIM25 expression (Fig. S4D). We also analyzed the association between the expression level of TRIM25 and the clinicopathological characteristics of BC patients. We found that the expression level of TRIM25 was notably correlated with tumor grade, tumor size, and muscle invasion (Table 1). In order to investigate the role of TRIM25 on BC cells, four specific shRNAs of TRIM25 were designed, and Western Blotting analysis showed that sh-TRIM25#3 and sh-TRIM25#4, but not sh-TRIM25#1 and sh-TRIM25#2, remarkably reduced the protein level of TRIM25 (Fig. 5H). After using sh-TRIM25#3 and sh-TRIM25#4 to knock down TRIM25, MDA and GSH levels in BC cells were examined. The results showed that MDA levels notably increased after TRIM25 expression was reduced (Fig. 5I), while GSH levels remarkably decreased (Fig. 5J). Moreover, we observed notably higher lipid peroxidation levels in the TRIM25 knockdown group than in the control group (Fig. 5K-M). TEM analysis revealed that the mitochondrial area of BC cells was remarkably reduced after TRIM25 knockdown (Fig. 5N-O). Meanwhile, After the silence of TRIM25, the levels of Fe²⁺ and ferroptosis markers TfR1 and ACSL4 in BC cells showed a significant increase (Figs. S4E-F). In addition, colony formation assay demonstrated that the proliferation capacity of BC cells in the TRIM25 knockdown group was notably lower than that in the control group (Fig. S4G). As indicated by the result of transwell assay, TRIM25 remarkably facilitated the migration and invasion of BC cells (Figs. S4H-I). These results demonstrate that TRIM25

not only inhibits ferroptosis in BC cells but also enhances their proliferation and invasion capabilities, making it a potential novel target for both diagnosis and treatment of BC.

3.7. TRIM25 inhibits ferroptosis in BC and plays a carcinogenic role

In order to further investigate the role of TRIM25 in BC, we synthesized an overexpression plasmid for TRIM25. We observed that, relative to the control group (Vector), the overexpression of TRIM25 significantly enhanced the proliferation (Fig. S5A), migration and invasion abilities (Fig. S5B) of BC cells. Additionally, the levels of MDA (Fig. S5C), Fe²⁺ (Fig. S5D), ACSL4, and TfR1 (Fig. S5E) were markedly reduced in BC cells with TRIM25 overexpression, while the GSH level (Fig. S5F) was significantly elevated. In line with this, lipid peroxidation levels were significantly reduced (Fig. S5G), and mitochondrial area was notably increased (Fig. S5H) in BC cells following TRIM25 overexpression. These results suggest that TRIM25 overexpression inhibits ferroptosis in BC cells, promoting their proliferation, invasion, and migration. Furthermore, in vivo experiments showed that the tumor growth rate (Fig. S5I), tumor volume (Fig. S5J), and tumor weight (Fig. S5K) of heterotopic subcutaneous xenograft tumors in mice were significantly lower after TRIM25 silencing compared to the control group, and these changes were opposite in the TRIM25 overexpression group. Additionally, results from a tail vein metastasis model indicated that TRIM25 promotes BC cell metastasis in vivo (Fig. S5L-N). Collectively, these findings suggest that TRIM25 suppresses ferroptosis in BC and plays a crucial pro-cancer role in the disease.

3.8. CTSGDP-13 effectively promotes the ferroptosis in BC by targeting TRIM25

To investigate whether CTSGDP-13 has a cancer-inhibiting role in BC by regulating TRIM25, rescue experiments were conducted. We constructed cell lines that stably overexpress TRIM25 (TRIM25) and control cell lines (Vector), and confirmed the efficiency of TRIM25 overexpression through Western Blotting analysis (Fig. 6A). After the overexpression of TRIM25, the elevated levels of MDA (Fig. 6B), Fe²⁺ (Fig. S6C), and ferroptosis-related markers (Fig. S6D) induced by CTSGDP-13 in BC cells significantly decreased. Conversely, the suppressed GSH levels in BC cells due to CTSGDP-13 exhibited a notable upswing (Fig. 6C). In addition, lipid peroxidation levels, which were increased by CTSGDP-13, were remarkably reduced after TRIM25 overexpression (Fig. 6D-F). Using TEM, we found that TRIM25 overexpression could notably recover the reduction of mitochondrial area caused by CTSGDP-13 (Fig. 6G and H). Moreover, the colony formation assay showed that the proliferation ability of BC cells inhibited by CTSGDP-13 was remarkably increased after TRIM25 overexpression (Fig. 6I). The Transwell assay indicated that TRIM25 overexpression could notably rescue the inhibition of CTSGDP-13 on the migration and invasion ability of BC cells (Fig. 6J, Fig. S6A). Western Blotting analysis showed that variations in the expression levels of markers related to migration and invasion in BC cells caused by CTSGDP-13, such as E-cadherin, N-cadherin, and Vimentin, were rescued by TRIM25 overexpression (Fig. S6B).

3.9. CTSGDP-13 regulated Keap1/NRF2 signaling pathway in BC

To identify the downstream target regulated by CTSGDP-13 in BC, proteomic sequencing was conducted. As depicted in Fig. 7A, compared with the Scr group, 606 differentially expressed proteins were identified in the CTSGDP-13 treatment group, with 180 up-regulated and 426 down-regulated (|fold change| > 1.2, P < 0.05). Radar plot shows the representative differentially expressed proteins (Fig. 7B). Among the above-mentioned dysregulated proteins, Kelch-like ECH-associated protein 1 (Keap1) drew the attention of our group for its remarkably elevated expression (Fig. 7C). Studies have shown that TRIM25 can

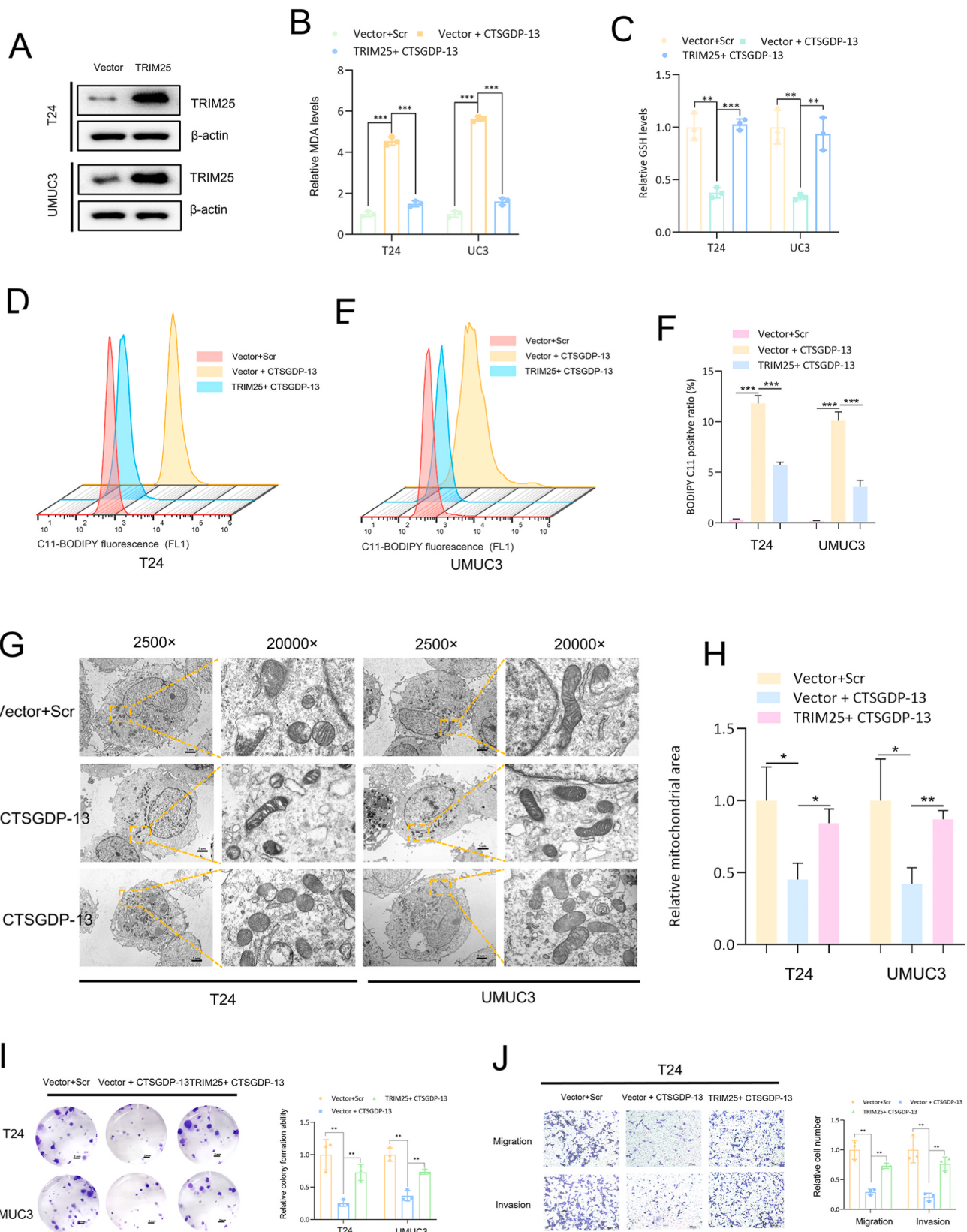
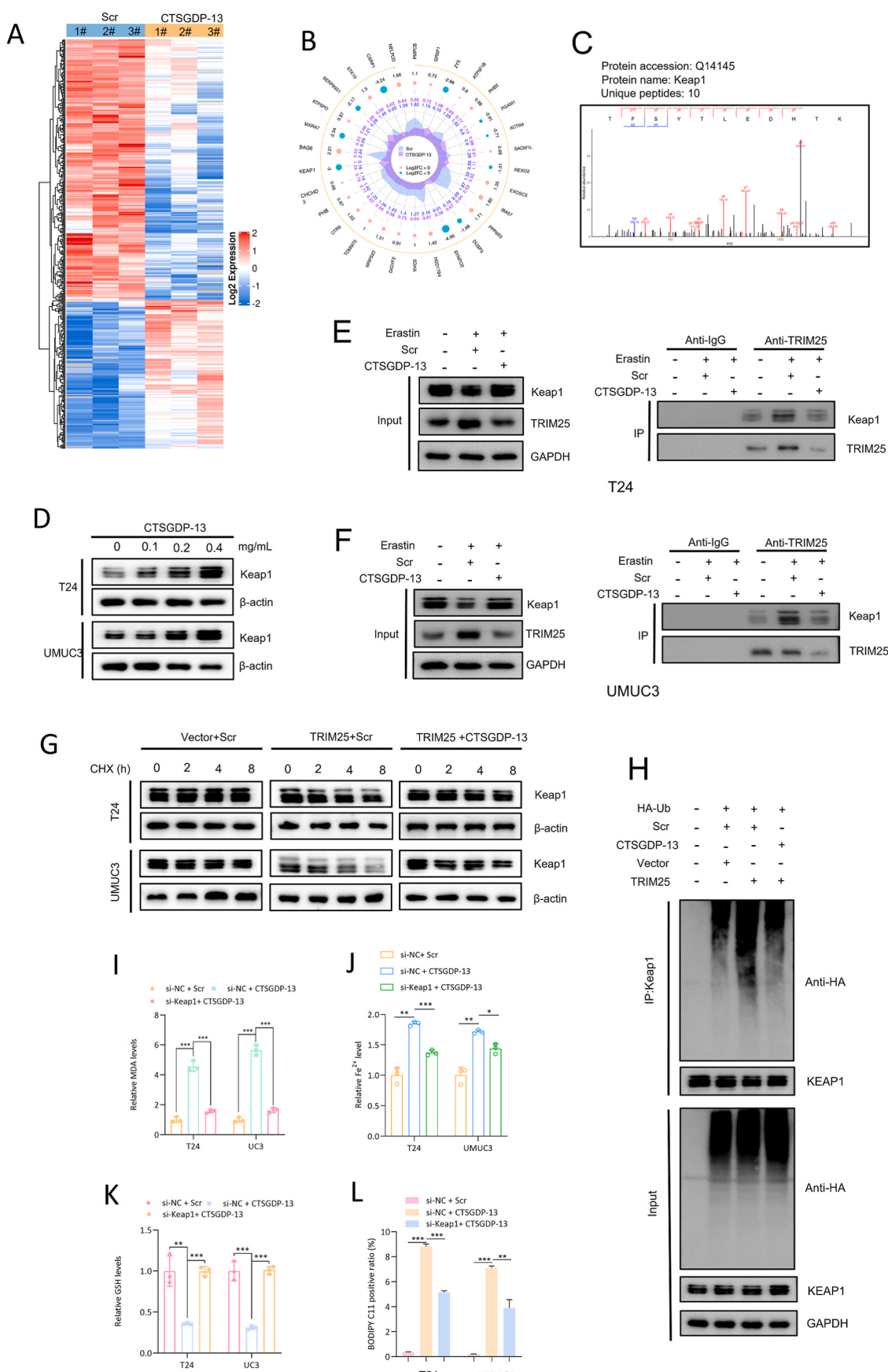


Fig. 6. CTSGDP-13 promotes ferroptosis in BC by inhibiting TRIM25. (A) Western blot analysis showing the TRIM25 level in BC cells after TRIM25 overexpression. (B) MDA levels in BC cells with different treatments. (C) GSH levels in BC cells with different treatments. The levels of lipid peroxidation in T24 cells (D) and UMUC3 cells (E) in each group were detected by C11-BODIPY probe. (F) Quantitative analysis of lipid peroxidation levels in BC cells. (G) Morphological changes of mitochondria of BC cells in each group observed by TEM. Scale bar: 5um. (H) Quantitative analysis of the mitochondrial area of BC cells observed in TEM (I) Colony formation assay showed the proliferation ability of BC cells after different treatments. Scale bar: 2 mm. (J) Transwell assay showed the migration and invasion capacities of T24 cells treated differently. Scale bar: 100um. *P < 0.05, **P < 0.01, ***P < 0.001.



(caption on next page)

Fig. 7. CTSGDP-13/TRIM25 regulated the progression of BC by regulating Keap1/NRF2 signaling pathway. (A) Heatmap showing differentially expressed proteins after CTSGDP-13 treatment. (B) Radar plot shows the representative differentially expressed proteins in CTSGDP-13 group. (C) Mass spectrum information of Keap1. (D) Western Blot analysis showed Keap1 levels in BC cells treated with different concentrations of CTSGDP-13. IP assay demonstrates the interaction between TRIM25 and Keap1 in T24 cells (E) and UMUC3 (F) cells. (G) Western Blot analysis showed the expression level of Keap1 in BC cells of each group after CHX treatment. (H) Western Blot analysis showing the ubiquitination level of keap1 of each group in T24 cells. (I) MDA levels in BC cells with different treatments. (J) Fe²⁺ levels in BC cells with different treatments. (K) GSH levels in BC cells with different treatments. (L) Detection of lipid peroxidation levels in each group using C11-BODIPY probe. *P < 0.05, **P < 0.01, ***P < 0.001.

promote Keap1 ubiquitination under endoplasmic reticulum (ER) stress, which has been proved to play a certain role in regulating ferroptosis [26]. In addition, Keap1 was found to regulate ferroptosis in multiple cancers [27,28]. Thus, we hypothesized that TRIM25 could regulate ferroptosis in BC cells by regulating Keap1 ubiquitination. Western Blotting analysis showed that the protein levels of Keap1 in BC cells increased with the addition of increasing doses of CTSGDP-13 (Fig. 7D). Furthermore, the co-IP assay results demonstrated a significant increase in the interaction between TRIM25 and Keap1 in BC cells upon the addition of Erastin, a ferroptosis inducer. In contrast, the interaction was remarkably reduced with the addition of CTSGDP-13 (Fig. 7E and F). To investigate the impact of CTSGDP-13/TRIM25 on Keap1 ubiquitination, we inhibited protein synthesis in BC cells by treating them with CHX. Western Blotting analysis revealed that TRIM25 notably facilitated the degradation of Keap1, whereas CTSGDP-13 hindered the effect of TRIM25 (Fig. 7G). Using Western Blotting analysis, we observed that TRIM25 remarkably facilitated Keap1 ubiquitination, while CTSGDP-13 rescued the elevated ubiquitination of Keap1 (Fig. 7H). Previous studies have confirmed that TRIM25 can regulate Keap1/NRF2 pathway by regulating Keap1 and inhibiting NRF2 nuclear translocation in ER stress [29]. Thus, using Western Blotting analysis, we found that CTSGDP-13 in BC cells could rescue the regulatory effect of TRIM25 on NRF2 nuclear translocation upon the addition of Erastin (Fig. S6A). While the regulatory effect of CTSGDP-13/TRIM25 on NRF2 nuclear translocation dismissed in the absent of Erastin (Fig. S6B). Keap1/NRF2 pathway has been confirmed to be closely related to BC progression [30,31]. We are interested in whether CTSGDP-13/TRIM25 regulates ferroptosis in BC cells by regulating Keap1 ubiquitination. We found that Keap1 knockdown could notably rescue the increase of MDA (Fig. 7I) and Fe²⁺ (Fig. 7J) level and the decrease of GSH (Fig. 7K) level induced by CTSGDP-13. Meanwhile, we found that Keap1 knockdown could rescue the lipid peroxidation levels increased by CTSGDP-13 in BC cells (Fig. 7L). Colony formation assay showed that the proliferation of BC cells inhibited by CTSGDP-13 was remarkably restored after Keap1 expression was reduced (Fig. S6C). Transwell assay revealed that Keap1 could notably reverse the inhibitory effect of CTSGDP-13 on the migration and invasion capacities of BC cells (Figs. S6D–E).

3.10. Overexpression of TRIM25 rescues the inhibitory effect of CTSGDP-13 on BC in vivo

We further investigated the effect of CTSGDP-13/TRIM25 on BC in vivo (Fig. 8A). In the subcutaneous xenograft tumor model, we observed that the tumor volume was remarkably lower in the “Vector + CTSGDP-13” group than in the “Vector + Scr” group. Additionally, the tumor volume was notably higher in the “TRIM25 + CTSGDP-13” group than in the “Vector + CTSGDP-13” group (Fig. 8B–G). We also noted that the tumor weight was remarkably lower in the “Vector + CTSGDP-13” group than in the “Vector + Scr” group, while the tumor quality was notably higher in the “TRIM25 + CTSGDP-13” group than in the “Vector + CTSGDP-13” group (Fig. 8H and I). H&E staining and IHC analysis were performed on tumor tissues in the respective group. We found that the expression levels of N-cadherin, Vimentin, TRIM25, and SLC7A11 in the “Vector + CTSGDP-13” group were considerably lower than those in the “Vector + Scr” and “TRIM25 + CTSGDP-13” groups. Conversely, the expression levels of E-cadherin and Keap1 in the “Vector + CTSGDP-13” group were remarkably higher than those in the “Vector + Scr” and “TRIM25 + CTSGDP-13” groups (Fig. 8J). In the tumor lung metastasis

model, we observed that the lung metastases of tumors in the “Vector + CTSGDP-13” group were notably less than those in the “Vector + Scr” and “TRIM25 + CTSGDP-13” groups (Fig. 9A and B). The above-mentioned findings indicate that CTSGDP-13 could effectively inhibit the growth and metastasis of BC in vivo, and the overexpression of TRIM25 could counteract this inhibitory effect.

3.11. CTSGDP-13 regulated BC ferroptosis by KEAP1/NRF2/SLC7A11 axis

SLC7A11 is a pivotal molecule that regulates ferroptosis. Previous studies have demonstrated that KEAP1 can decrease the expression of SLC7A11, thereby promoting the ferroptosis of cancer cells [32]. Accordingly, we analyzed whether CTSGDP-13 can promote ferroptosis of BC cells by modulating SLC7A11. Western Blotting analysis showed that CTSGDP-13 reduced SLC7A11 expression in a dose-dependent manner (Fig. 9C). We constructed an overexpression plasmid of SLC7A11, and Western Blotting analysis confirmed that SLC7A11 overexpression remarkably restored the reduction of SLC7A11 caused by CTSGDP-13 (Fig. 9D). We found that overexpression of SLC7A11 could notably restore the MDA level increased by CTSGDP-13 in BC cells (Fig. 9E). The detection of GSH level found that overexpression of SLC7A11 could remarkably restore the GSH level reduced by CTSGDP-13 in BC cells (Fig. 9F). Meanwhile, lipid peroxidation levels, which were increased by CTSGDP-13, were notably decreased after SLC7A11 overexpression (Fig. 9G). Colony formation assay showed that overexpression of SLC7A11 could significantly restore the proliferation capacity inhibited by CTSGDP-13 in BC (Fig. 9H). Transwell assay showed that the migration and invasion abilities of BC cells, which were inhibited by CTSGDP-13, were significantly increased after SLC7A11 overexpression (Fig. 9I). The above-described results indicated that CTSGDP-13 regulated BC ferroptosis by regulating SLC7A11.

4. Discussion

The endogenous peptide CTSGDP-13 originates from Cathepsin G, a member of the neutrophil serine protease family, which is notable for its pathogenic killing effect [33]. Several peptides derived from Cathepsin G have been reported with pathogen-inhibiting activity similar to its precursor protein [34–36]. However, Cathepsin G plays a certain role in the regulation of various diseases [33,37,38]. In 2008, Thomas J Wilson et al. found that Cathepsin G could enhance mammary tumor-induced osteolysis by generating soluble receptor activator of nuclear factor-kappaB ligand [39]. Furthermore, a novel peptide derived from Cathepsin G was identified as a target in acute myeloid leukemia [40]. Thus, when the significantly down-regulated expression of CTSGDP-13 in BC was observed, we anticipated that it could exert an anti-tumor effect similar to its precursor protein in BC. Interestingly, we treated BC cells with CTSGDP-13 and found that it inhibited proliferation, invasion, and migration while promoting ferroptosis.

Since existing research on ferroptosis has become more extensive over the past few years, its crucial role in regulating cancer has been revealed [14,41]. Previous studies have confirmed that ferroptosis plays a certain role in regulating hepatocellular carcinoma, colorectal cancer, gastric cancer, and other cancers through multiple mechanisms, including malignant progression, tumor drug resistance, and immune evasion [42]. In BC, Liang et al. found that MAFG-AS1 could contribute to cisplatin resistance through antagonistic ferroptosis [43].

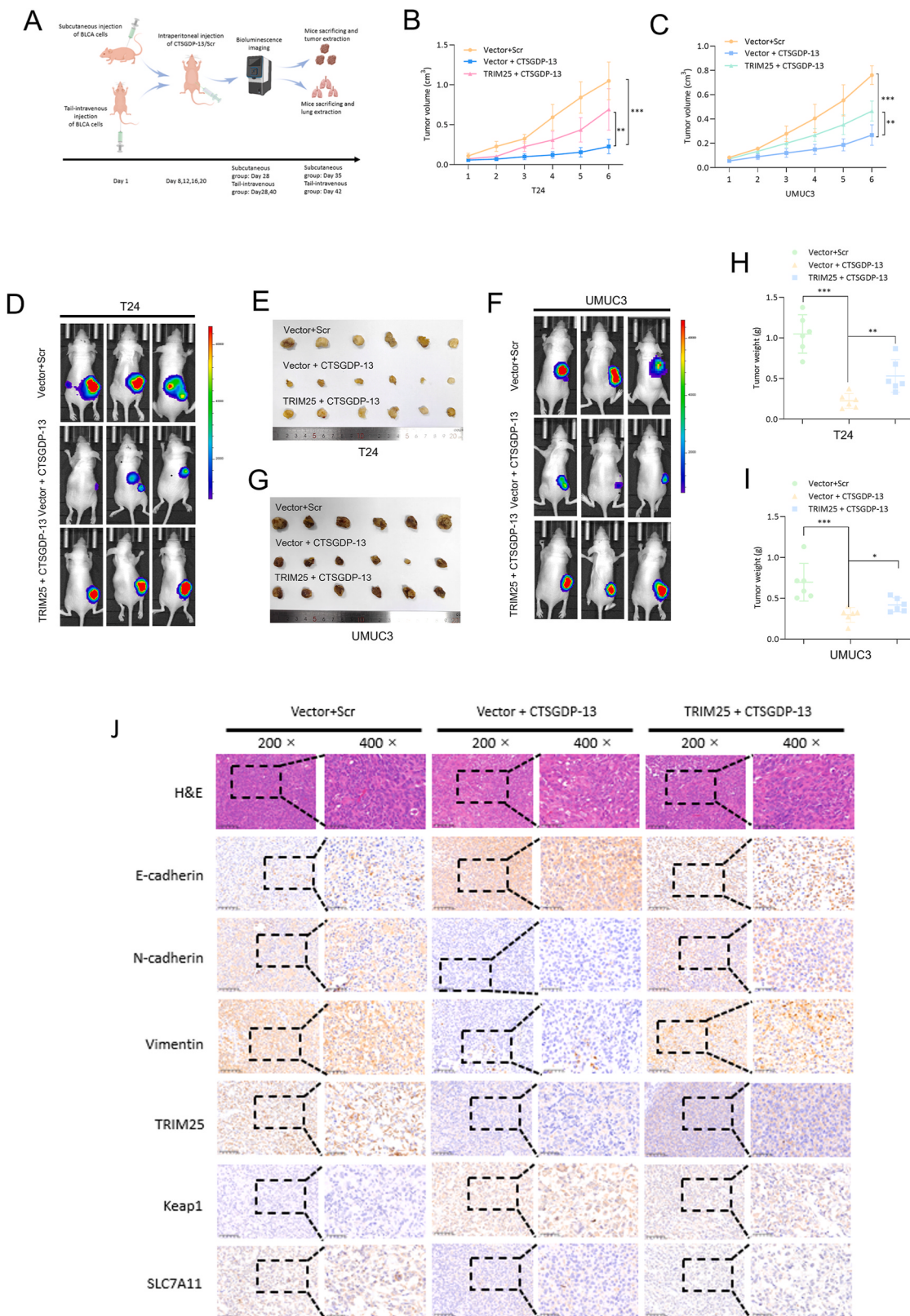


Fig. 8. CTSGDP-13 inhibits BC progression in vivo by regulating TRIM25. (A) Flow chart of animal study. (B) Subcutaneous tumor volume of mice injected with T24 cells of each group. (C) Subcutaneous tumor volume of mice injected with UMUC3 cells of each group. (D) The tumor growth in mice injected T24 cells was analyzed using In Vivo Imaging System. (E) The tumor in mice injected differentially treated T24 cells. (F) The tumor growth in mice injected UMUC3 cells was analyzed using In Vivo Imaging System (G) The tumor in mice injected differentially treated UMUC3 cells. (H) Tumor weight in mice injected differentially treated T24 cells. (I) Tumor weight in mice injected differentially treated UMUC3 cells. (J) Mice tumor tissues were analyzed by H&E and IHC. Scale bar: 100um. *P < 0.05, **P < 0.01, ***P < 0.001.

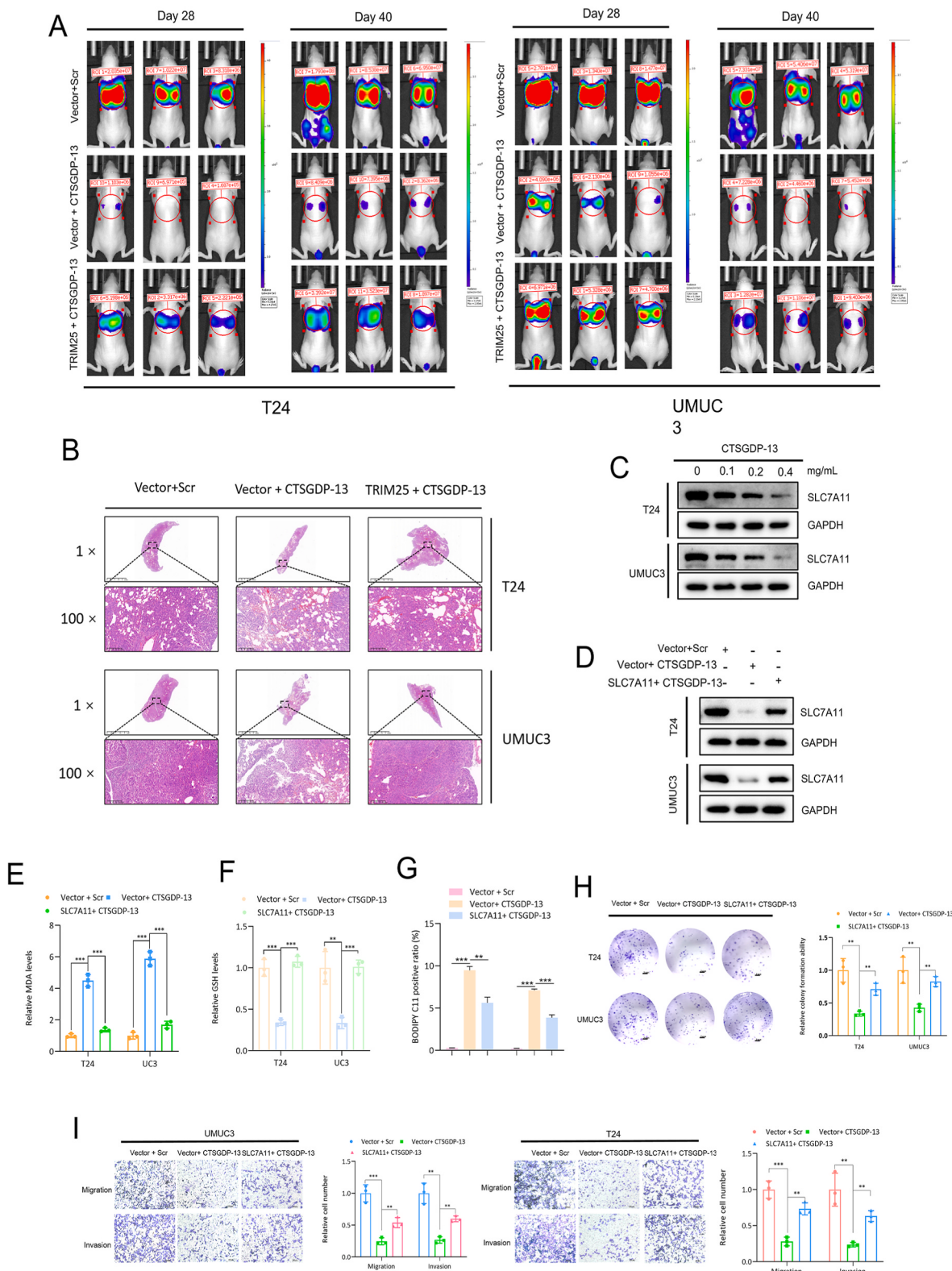


Fig. 9. CTSGDP-13 inhibits the ferroptosis of BC by regulating SLC7A11. (A) The lung metastasis growth in mice injected BC cells was analyzed using In Vivo Imaging System. (B) Slides of lungs by hematoxylin and eosin-stained. (C) Western blot analysis was conducted to assess the expression levels of SLC7A11 after exposure to varying concentrations of CTSGDP-13. (D) Western blot analysis showed the expression levels of SLC7A11 in different group of BC cells. (E) MDA levels in BC cells were assessed following different treatments. (F) GSH levels in BC cells with different treatments. (G) Lipid peroxidation levels in each group were detected using the C11-BODIPY probe. (H) Colony formation assay showed the proliferation ability of BC cells in each group. Scale bar: 2 mm. (I) Transwell assay shows the migration and invasion abilities of differently treated BC cells. Scale bar: 100μm. *P < 0.05, **P < 0.01, ***P < 0.001.

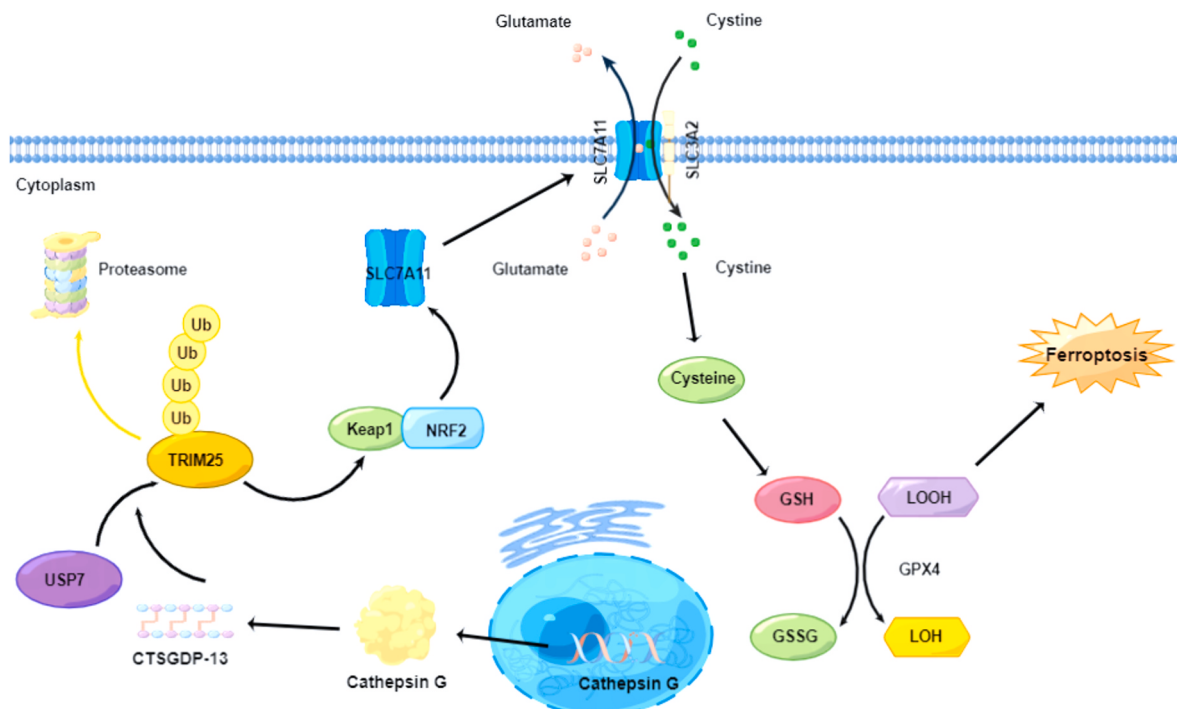


Fig. 10. Schematic diagram illustrating how CTSGDP-13 promotes ferroptosis in BC by regulating TRIM25/Keap1/NRF2/SLC7A11 axis.

Fin56-induced ferroptosis was reported to be supported by autophagy-mediated GPX4 degradation and functioned synergistically with mTOR inhibition to kill BC cells [44]. Furthermore, Liu et al. developed iron-containing protein-mimetic supramolecular iron delivery systems for ferroptosis-based tumor therapy [45]. Excitingly, CTSGDP-13 has been found to promote ferroptosis in BC. Accordingly, we investigated the mechanism by which it regulates ferroptosis in BC.

The tripartite motif (TRIM) protein family takes on critical significance in cell differentiation, autophagy, apoptosis, DNA repair, and tumor suppression through its ubiquitination activity as E3 ligase [46]. TRIM25 (i.e., estrogen response finger protein) has been first recognized for its estrogen-inducing effect [47]. TRIM25, a member of the TRIM protein family and an E3 ligase, is vital to antiviral innate immunity, growth and development, tumor progression, and other areas [48,49]. Extensive research has suggested the biphasic regulation of TRIM25 in cancer. On the one hand, TRIM25 promotes the progression of breast cancer [50], prostate cancer [51], hepatocellular carcinoma [29], colorectal cancer [52], non-small cell lung cancer [53]. On the other hand, TRIM25 plays a significant role as a tumor suppressor in gastric cancer [54,55]. Although previous research has reported that TRIM25 plays a certain role in BC regulation as an E3 ligase [56], the role played by TRIM25 in BC has not been thoroughly investigated. In this study, the result of bioinformatics analysis confirmed that the expression level of TRIM25 was up-regulated in BC and correlated with poor prognosis of BC patients. Furthermore, the results confirmed that TRIM25, a downstream protein of CTSGDP-13, can facilitate BC progression by inhibiting ferroptosis *in vitro* and *in vivo*.

The mechanism of how CTSGDP-13/TRIM25 regulates ferroptosis arouses our interest. Ferroptosis is correlated with two vital biochemical features (i.e., iron accumulation and lipid peroxidation) [57]. The system XC₋, comprising SLC7A11 and SLC3A2, maintains GSH production, such that lipid peroxidation in cells can be prevented [15]. Existing studies have demonstrated that inhibition of the SLC7A11 pathway serves as one of the most critical upstream mechanisms for the induction of ferroptosis [13]. This study suggested that CTSGDP-13 is capable of remarkably down-regulating the protein level of SLC7A11. Proteomics sequencing was conducted to explore the downstream targets of

CTSGDP-13/TRIM25 regulation. Keap1 in the CTSGDP-13 group aroused the attention of our group for its notably up-regulated expression level compared with the control group. As revealed by previous research, TRIM25 is capable of facilitating HCC progression by targeting the Keap1-Nrf2 pathway [29]. The Keap1-Nrf2 pathway has been confirmed to play a regulatory role on SLC7A11 in ferroptosis [58,59]. Our subsequent experiments confirmed that CTSGDP-13/TRIM25 is capable of regulating the expression level of SLC7A11 through the Keap1-Nrf2 pathway, such that it can facilitate ferroptosis in BC cells while serving as a cancer suppressor.

CTSGDP-13, an endogenous short peptide, is enzymatically cleaved from its precursor protein by Cathepsin G. Investigating the upstream regulatory mechanisms of CTSGDP-13 in the progression of BC is of paramount significance for elucidating the core regulatory pathways associated with this peptide. However, the current lack of quantitative analysis methods for CTSGDP-13 poses challenges in exploring its generation mechanisms. Simultaneously, we will persist in future efforts to develop more suitable quantitative analysis methods for CTSGDP-13, aiming to unveil its clinical value as a diagnostic biomarker. Nevertheless, certain limitations in this study must be acknowledged. Firstly, we encountered deficiencies in control groups during the study design phase, such as neglecting the impact of DFO on ferroptosis levels in the Scr group BC cells. Additionally, in rescue experiments, we did not investigate the effects of Keap1 silencing and SLC7A11 overexpression solely on the malignant phenotype of BC cells. Despite our confidence that the roles of DFO, Keap1, and SLC7A11 in ferroptosis and BC have been confirmed, and the absence of these control groups does not compromise the conclusions of this study, the design flaws in these experiments do, to some extent, diminish the rigor of our research.

5. Conclusion

In this study, 128 endogenous peptides notably differentially expressed in BC were identified. CTSGDP-13, a novel peptide derived from Cathepsin G, has aroused the attention of our group for its potential cancer suppressive effect. As indicated by the result of this study, CTSGDP-13 can facilitate the ferroptosis in BC by disrupting the

interaction between deubiquitinase USP7 and TRIM25 and regulating the TRIM25/KEAP1/NRF2 axis. (Fig. 10). The in-depth research on the roles of CTSGDP-13 and TRIM25 in BC can help provide promising paths for the development of new diagnostic and therapeutic targets for BC.

Ethics approval and consent to participate

The collection of human tissue samples conformed to the Declaration of Helsinki and gained approval from the Board and Ethics Committee of Huashan Hospital, Fudan University (No. KY2011-009). Each patient provided written informed consent before tissue samples were collected. The animal experiments were approved by the Board and Ethics Committee of Huashan Hospital, Fudan University.

Consent for publication

Not applicable.

Availability of data and material

The datasets used and/or analyzed during the present study are available from the corresponding author on reasonable request.

Funding

This work was supported by the National Natural Science Foundation of China (No.81802569, 82273014, 82373222, 82103215), Leading Talent Program by Shanghai Municipal Health Commission (2022LJ008), Medical Innovation Research Special Project by Science and Technology Commission of Shanghai Municipality (22Y21900200), Clinical Scientific and Technological Innovation Project by Shanghai Hospital Development Center (SHDC12021104).

CRediT authorship contribution statement

Weijian Li: Conceptualization. **Ye Shen:** Conceptualization. **Chen Yang:** Data curation, Funding acquisition. **Fangdie Ye:** Formal analysis. **Yingchun Liang:** Formal analysis. **Zhang Cheng:** Investigation. **Yuxi Ou:** Methodology, Investigation. **Wensun Chen:** Supervision. **Ziang Chen:** Investigation. **Lujia Zou:** Validation. **Yufei Liu:** Software. **Yun Hu:** Visualization. **Xiang Yan:** Funding acquisition, Writing – review & editing, Writing – original draft. **Haowen Jiang:** Methodology, Investigation, Funding acquisition.

Declaration of competing interest

The authors declare that they have no known competing financial interests or personal relationships that could have appeared to influence the work reported in this paper.

Acknowledgements

Not applicable.

Abbreviations

BC	Bladder cancer
NMIBC	non-muscular invasive bladder cancer
MIBC	muscular invasive bladder cancer
CTSGDP-13	Cathepsin G Derived Peptide-13
GSH	glutathione
GPX4	glutathione peroxidase 4
PLOOHs	phospholipid hydroperoxides
TMT	tandem mass tag
LC-MS/MS	Liquid Chromatography-Mass Spectrometry/Mass Spectrometry

MDA	Malondialdehyde
TBA	thiobarbituric acid
IHC	immunohistochemistry
DMSO	Dimethyl Sulfoxide
FBS	fetal bovine serum
CCK-8	Cell Counting Kit-8
qRT-PCR	RNA extraction and quantitative real-time PCR
WB	Western blot
ROS	Reactive Oxygen Species
TEM	transmission electron microscopy
TCGA	The Cancer Genome Atlas
FDR	false discovery rate
KEGG	Kyoto Encyclopedia of Genes and Genomes
PVDF	polyvinylidene difluoride
ECL	enhanced chemiluminescence
SDS-PAGE	Sodium Dodecyl Sulfate Polyacrylamide Gel Electrophoresis
DFO	Desferrioxamine
CQ	Chloroquine
NAC	N-acetylcysteine
CHX	Cycloheximide
CC	coiled-coil
PS	PRY/SPRY
PCA	Principal Component Analysis
PFI	progression free interval
ER	endoplasmic reticulum
TRIM	tripartite motif

Appendix A. Supplementary data

Supplementary data to this article can be found online at <https://doi.org/10.1016/j.canlet.2023.216515>.

References

- [1] F. Bray, J. Ferlay, I. Soerjomataram, R.L. Siegel, L.A. Torre, A. Jemal, Global cancer statistics 2018: GLOBOCAN estimates of incidence and mortality worldwide for 36 cancers in 185 countries, CA Cancer J Clin 68 (2018) 394–424.
- [2] S. Li, K. Xin, S. Pan, Y. Wang, J. Zheng, Z. Li, X. Liu, B. Liu, Z. Xu, X. Chen, Blood-based liquid biopsy: insights into early detection, prediction, and treatment monitoring of bladder cancer, Cell. Mol. Biol. Lett. 28 (2023) 28.
- [3] C. Yang, Z. Mou, Z. Zhang, S. Wu, Q. Zhou, Y. Chen, J. Gong, C. Xu, Y. Ou, X. Chen, X. Dai, H. Jiang, Circular RNA RBPM5 inhibits bladder cancer progression via miR-330-3p/RAI2 regulation, Mol. Ther. Nucleic Acids 23 (2021) 872–886.
- [4] M.A. Knowles, C.D. Hurst, Molecular biology of bladder cancer: new insights into pathogenesis and clinical diversity, Nat. Rev. Cancer 15 (2015) 25–41.
- [5] V.G. Patel, W.K. Oh, M.D. Galsky, Treatment of muscle-invasive and advanced bladder cancer in 2020, CA Cancer J Clin 70 (2020) 404–423.
- [6] S. Jiang, J. Wang, C. Yang, R. Tan, J. Hou, Y. Shi, H. Zhang, S. Ma, J. Wang, M. Zhang, G. Phillips, Z. Li, J. Ma, W. Yu, G. Wang, Y. Wu, R. Schlegel, H. Wang, S. Cao, J. Guo, X. Liu, Y. Dang, Continuous culture of urine-derived bladder cancer cells for precision medicine, Protein Cell 10 (2019) 902–907.
- [7] F. Arasteh, K. Abnous, M. Hashemi, S.M. Taghdisi, M. Ramezani, M. Alibolandi, Peptide-based targeted therapeutics: focus on cancer treatment, J Control Release 292 (2018) 141–162.
- [8] K.N. Sugahara, T. Teesalu, P.P. Karmali, V.R. Kotamraju, L. Agemy, O.M. Girard, D. Hanahan, R.F. Mattrey, E. Ruoslahti, Tissue-penetrating delivery of compounds and nanoparticles into tumors, Cancer Cell 16 (2009) 510–520.
- [9] S. Annett, G. Moore, A. Short, A. Marshall, C. McCrudden, A. Yakkundi, S. Das, W. G. McCluggage, L. Nelson, I. Harley, N. Moustafa, C.J. Kennedy, A. deFazio, A. Brand, R. Sharma, D. Brennan, S. O'Toole, J. O'Leary, M. Bates, C. O'Riain, D. O'Connor, F. Furlong, H. McCarthy, A. Kisselkennig, L. McClements, T. Robson, FKBP1-based peptide, ALM201, targets angiogenesis and cancer stem cells in ovarian cancer, Br. J. Cancer 122 (2020) 361–371.
- [10] L. Nannan, W. Gsell, S. Belderbos, C. Gallet, J. Wouters, S. Brassart-Pasco, U. Himmelreich, B. Brassart, A multimodal imaging study to highlight elastin-derived peptide pro-tumoral effect in a pancreatic xenograft model, Br. J. Cancer 128 (2023) 2000–2012.
- [11] K. Desai, J.M. McManus, N. Sharifi, Hormonal therapy for prostate cancer, Endocr. Rev. 42 (2021) 354–373.
- [12] S.J. Dixon, K.M. Lemberg, M.R. Lamprecht, R. Skouta, E.M. Zaitsev, C.E. Gleason, D.N. Patel, A.J. Bauer, A.M. Cantley, W.S. Yang, B. Morrison 3rd, B.R. Stockwell, Ferroptosis: an iron-dependent form of nonapoptotic cell death, Cell 149 (2012) 1060–1072.
- [13] D. Tang, X. Chen, R. Kang, G. Kroemer, Ferroptosis: molecular mechanisms and health implications, Cell Res. 31 (2021) 107–125.

- [14] X. Chen, R. Kang, G. Kroemer, D. Tang, Broadening horizons: the role of ferroptosis in cancer, *Nat. Rev. Clin. Oncol.* 18 (2021) 280–296.
- [15] X. Jiang, B.R. Stockwell, M. Conrad, Ferroptosis: mechanisms, biology and role in disease, *Nat. Rev. Mol. Cell Biol.* 22 (2021) 266–282.
- [16] X. Chen, J. Li, R. Kang, D.J. Klionsky, D. Tang, Ferroptosis: machinery and regulation, *Autophagy* 17 (2021) 2054–2081.
- [17] B. Hassannia, P. Vandenebeele, T. Vanden Berghe, Targeting ferroptosis to iron out cancer, *Cancer Cell* 35 (2019) 830–849.
- [18] Y. Wang, L. Zheng, W. Shang, Z. Yang, T. Li, F. Liu, W. Shao, L. Lv, L. Chai, L. Qu, Q. Xu, J. Du, X. Liang, J. Zeng, J. Jia, Wnt/beta-catenin signaling confers ferroptosis resistance by targeting GPX4 in gastric cancer, *Cell Death Differ.* 29 (2022) 2190–2202.
- [19] X. Wang, Y. Chen, X. Wang, H. Tian, Y. Wang, J. Jin, Z. Shan, Y. Liu, Z. Cai, X. Tong, Y. Luan, X. Tan, B. Luan, X. Ge, H. Ji, X. Jiang, P. Wang, Stem cell factor SOX2 confers ferroptosis resistance in lung cancer via upregulation of SLC7A11, *Cancer Res.* 81 (2021) 5217–5229.
- [20] J. Yang, Y. Zhou, S. Xie, J. Wang, Z. Li, L. Chen, M. Mao, C. Chen, A. Huang, Y. Chen, X. Zhang, N.U.H. Khan, L. Wang, J. Zhou, Metformin induces Ferroptosis by inhibiting UFMylation of SLC7A11 in breast cancer, *J. Exp. Clin. Cancer Res.* 40 (2021) 206.
- [21] C. Yang, S. Wu, Z. Mou, Q. Zhou, X. Dai, Y. Ou, X. Chen, Y. Chen, C. Xu, Y. Hu, L. Zhang, L. Zou, S. Jin, J. Hu, S. Mao, H. Jiang, Exosome-derived circTRPS1 promotes malignant phenotype and CD8+ T cell exhaustion in bladder cancer microenvironments, *Mol. Ther.* 30 (2022) 1054–1070.
- [22] W. Li, Y. Li, W. Ma, J. Zhou, Z. Sun, X. Yan, Long noncoding RNA AC114812.8 promotes the progression of bladder cancer through miR-371b-5p/FUT4 axis, *Biomed. Pharmacother.* 121 (2020), 109605.
- [23] X. Wu, J. Zhou, L. Zhao, Z. Yang, C. Yang, Y. Chen, W. Xue, CircCYP24A1 hampered malignant phenotype of renal cancer carcinoma through modulating CMTM-4 expression via sponging miR-421, *Cell Death Dis.* 13 (2022) 190.
- [24] C. Yang, S. Wu, X. Wu, X. Zhou, S. Jin, H. Jiang, Silencing circular RNA UVRAG inhibits bladder cancer growth and metastasis by targeting the microRNA-223/fibroblast growth factor receptor 2 axis, *Cancer Sci.* 110 (2019) 99–106.
- [25] Z. Cheng, H. Zhang, L. Zhang, X. Wang, Q. Zhang, M. Feng, D. Hu, H. Li, L. Qian, Exercise-induced peptide TAG-23 protects cardiomyocytes from reperfusion injury through regulating PKG-Cbl interaction, *Basic Res. Cardiol.* 116 (2021) 41.
- [26] F. Fu, W. Wang, L. Wu, W. Wang, Z. Huang, Y. Huang, C. Wu, X. Pan, Inhalable biomimetic liposomes for cyclic Ca(2+)-burst-centered endoplasmic reticulum stress enhanced lung cancer ferroptosis therapy, *ACS Nano* 17 (2023) 5486–5502.
- [27] C.A. Wohlhieter, A.L. Richards, F. Uddin, C.H. Hulton, A. Quintanal-Villalonga, A. Martin, E. de Stanchina, U. Bhanot, M. Asher, N.S. Shah, O. Hayatt, D. J. Buonocore, N. Rekhtman, R. Shen, K.C. Arbour, M. Donoghue, J.T. Poirier, T. Sen, C.M. Rudin, Concurrent mutations in STK11 and KEAP1 promote ferroptosis protection and SCD1 dependence in lung cancer, *Cell Rep.* 33 (2020), 108444.
- [28] X. Sun, Z. Ou, R. Chen, X. Niu, D. Chen, R. Kang, D. Tang, Activation of the p62-Keap1-NRF2 pathway protects against ferroptosis in hepatocellular carcinoma cells, *Hepatology* 63 (2016) 173–184.
- [29] Y. Liu, S. Tao, L. Liao, Y. Li, H. Li, Z. Li, L. Lin, X. Wan, X. Yang, L. Chen, TRIM25 promotes the cell survival and growth of hepatocellular carcinoma through targeting Keap1-Nrf2 pathway, *Nat. Commun.* 11 (2020) 348.
- [30] M.A. Cucci, M. Grattarola, C. Dianzani, G. Damia, F. Ricci, A. Roetto, F. Trotta, G. Barrera, S. Pizzimenti, Ailanthon increases oxidative stress in CDDP-resistant ovarian and bladder cancer cells by inhibiting of Nrf2 and YAP expression through a post-translational mechanism, *Free Radic. Biol. Med.* 150 (2020) 125–135.
- [31] M. Hayashi, E. Guida, Y. Inokawa, R. Goldberg, L.O. Reis, A. Ooki, M. Pilli, P. Sadhukhan, J. Woo, W. Choi, E. Izumchenko, L.M. Gonzalez, L. Marchionni, A. Zhavoronkov, M. Brait, T. Bivalacqua, A. Baras, G.J. Netto, W. Koch, A. Singh, M.O. Hoque, GULP1 regulates the NRF2-KEAP1 signalling axis in urothelial carcinoma, *Sci. Signal.* 13 (2020).
- [32] Z. Fan, A.K. Wirth, D. Chen, C.J. Wruck, M. Rauh, M. Buchfelder, N. Savaskan, Nrf2-Keap1 pathway promotes cell proliferation and diminishes ferroptosis, *Oncogenesis* 6 (2017) e371.
- [33] S. Gao, H. Zhu, X. Zuo, H. Luo, Cathepsin G and its role in inflammation and autoimmune diseases, *Arch. Rheumatol.* 33 (2018) 498–504.
- [34] W.M. Shafer, S. Katzfif, S. Bowers, M. Fallon, M. Hubalek, M.S. Reed, P. Veprek, J. Pohl, Tailoring an antibacterial peptide of human lysosomal cathepsin G to enhance its broad-spectrum action against antibiotic-resistant bacterial pathogens, *Curr. Pharm. Des.* 8 (2002) 695–702.
- [35] K.T. Miyasaki, A.L. Bodeau, J. Pohl, W.M. Shafer, Bactericidal activities of synthetic human leukocyte cathepsin G-derived antibiotic peptides and congeners against *Actinobacillus actinomycetemcomitans* and *Campylobacter jejuni*, *Antimicrob. Agents Chemother.* 37 (1993) 2710–2715.
- [36] W.M. Shafer, J. Pohl, V.C. Onunkwa, N. Bangalore, J. Travis, Human lysosomal cathepsin G and granzyme B share a functionally conserved broad spectrum antibacterial peptide, *J. Biol. Chem.* 266 (1991) 112–116.
- [37] T. Burster, U. Knippschild, F. Molnár, A. Zhanapiya, Cathepsin G and its dichotomous role in modulating levels of MHC class I molecules, *Arch. Immunol. Ther. Exp.* 68 (2020) 25.
- [38] T. Burster, H. Macmillan, T. Hou, B.O. Boehm, E.D. Mellins, Cathepsin G: roles in antigen presentation and beyond, *Mol. Immunol.* 47 (2010) 658–665.
- [39] T.J. Wilson, K.C. Nannuru, M. Futakuchi, A. Sadanandam, R.K. Singh, Cathepsin G enhances mammary tumor-induced osteolysis by generating soluble receptor activator of nuclear factor-kappaB ligand, *Cancer Res.* 68 (2008) 5803–5811.
- [40] M. Zhang, P. Sukhumalchandra, A.A. Enyenohi, L.S. St John, S.A. Hunsucker, E. A. Mittendorf, A. Sergeeva, K. Ruisaard, Z. Al-Atrache, P.A. Ropp, H. Jakher, T. Rodriguez-Cruz, G. Lizee, K. Clise-Dwyer, S. Lu, J.J. Moledrem, G.L. Glish, P. M. Armistead, G. Alatrash, A novel HLA-A*0201 restricted peptide derived from cathepsin G is an effective immunotherapeutic target in acute myeloid leukemia, *Clin. Cancer Res.* 19 (2013) 247–257.
- [41] G. Lei, L. Zhuang, B. Gan, Targeting ferroptosis as a vulnerability in cancer, *Nat. Rev. Cancer* 22 (2022) 381–396.
- [42] Y. Mou, J. Wang, J. Wu, D. He, C. Zhang, C. Duan, B. Li, Ferroptosis, a new form of cell death: opportunities and challenges in cancer, *J. Hematol. Oncol.* 12 (2019) 34.
- [43] L. Xiang, Q. Zeng, J. Liu, M. Xiao, D. He, Q. Zhang, D. Xie, M. Deng, Y. Zhu, Y. Liu, H. Bo, X. Liu, M. Zhou, W. Xiong, Y. Zhou, J. Zhou, X. Li, K. Cao, MAFG-AS1/MAFG positive feedback loop contributes to cisplatin resistance in bladder urothelial carcinoma through antagonistic ferroptosis, *Sci. Bull.* 66 (2021) 1773–1788.
- [44] Y. Sun, N. Berleth, W. Wu, D. Schluetermann, J. Deitersen, F. Stuhldreier, L. Berning, A. Friedrich, S. Akgün, M.J. Mendiburo, S. Wesselborg, M. Conrad, C. Berndt, B. Stork, Fin56-induced ferroptosis is supported by autophagy-mediated GPX4 degradation and functions synergistically with mTOR inhibition to kill bladder cancer cells, *Cell Death Dis.* 12 (2021) 1028.
- [45] S. Liu, M. Zhang, H. Jin, Z. Wang, Y. Liu, S. Zhang, H. Zhang, Iron-containing protein-mimic supramolecular iron delivery systems for ferroptosis tumor therapy, *J. Am. Chem. Soc.* 145 (2023) 160–170.
- [46] F.P. Williams, K. Haubrich, C. Perez-Borrero, J. Hennig, Emerging RNA-binding roles in the TRIM family of ubiquitin ligases, *Biol. Chem.* 400 (2019) 1443–1464.
- [47] T. Urano, T. Saito, T. Tsukui, M. Fujita, T. Hosoi, M. Muramatsu, Y. Ouchi, S. Inoue, Efp targets 14-3-3 sigma for proteolysis and promotes breast tumour growth, *Nature* 417 (2002) 871–875.
- [48] M. Martín-Vicente, L.M. Medrano, S. Resino, A. García-Sastre, I. Martínez, TRIM25 in the regulation of the antiviral innate immunity, *Front. Immunol.* 8 (2017) 1187.
- [49] G. Heikel, N.R. Choudhury, G. Michlewski, The role of Trim25 in development, disease and RNA metabolism, *Biochem. Soc. Trans.* 44 (2016) 1045–1050.
- [50] L.A. Walsh, M.J. Alvarez, E.Y. Sabio, M. Reyngold, V. Makarov, S. Mukherjee, K. W. Lee, A. Desrichard, S. Turcan, M.G. Dalton, V.K. Rajasekhar, S. Chen, L. T. Vahdat, A. Califano, T.A. Chan, An integrated systems biology approach identifies TRIM25 as a key determinant of breast cancer metastasis, *Cell Rep.* 20 (2017) 1623–1640.
- [51] K.I. Takayama, T. Suzuki, T. Tanaka, T. Fujimura, S. Takahashi, T. Urano, K. Ikeda, S. Inoue, TRIM25 enhances cell growth and cell survival by modulating p53 signals via interaction with G3BP2 in prostate cancer, *Oncogene* 37 (2018) 2165–2180.
- [52] S. Zhou, J. Peng, L. Xiao, C. Zhou, Y. Fang, Q. Ou, J. Qin, M. Liu, Z. Pan, Z. Hou, TRIM25 regulates oxaliplatin resistance in colorectal cancer by promoting EZH2 stability, *Cell Death Dis.* 12 (2021) 463.
- [53] Y.M. He, X.M. Zhou, S.Y. Jiang, Z.B. Zhang, B.Y. Cao, J.B. Liu, Y.Y. Zeng, J. Zhao, X.L. Mao, TRIM25 activates AKT/mTOR by inhibiting PTEN via K63-linked polyubiquitination in non-small cell lung cancer, *Acta Pharmacol. Sin.* 43 (2022) 681–691.
- [54] J.J. Chen, Y.L. Ren, C.J. Shu, Y. Zhang, M.J. Chen, J. Xu, J. Li, A.P. Li, D.Y. Chen, J. D. He, Y.Q. Shu, J.W. Zhou, JP3, an antiangiogenic peptide, inhibits growth and metastasis of gastric cancer through TRIM25/SPI1/MMP2 axis, *J. Exp. Clin. Cancer Res.* 39 (2020) 118.
- [55] X. Zang, J. Jiang, J. Gu, Y. Chen, M. Wang, Y. Zhang, M. Fu, H. Shi, H. Cai, H. Qian, W. Xu, X. Zhang, Circular RNA EIF4G3 suppresses gastric cancer progression through inhibition of β -catenin by promoting δ -catenin ubiquitin degradation and upregulating SIK1, *Mol. Cancer* 21 (2022) 141.
- [56] H. Tang, X. Li, L. Jiang, Z. Liu, L. Chen, J. Chen, M. Deng, F. Zhou, X. Zheng, Z. Liu, RITA1 drives the growth of bladder cancer cells by recruiting TRIM25 to facilitate the proteasomal degradation of RBPJ, *Cancer Sci.* 113 (2022) 3071–3084.
- [57] D. Li, Y. Li, The interaction between ferroptosis and lipid metabolism in cancer, *Signal Transduct Target Ther.* 5 (2020) 108.
- [58] S. Bader, J. Wilmers, M. Pelzer, V. Jendrossek, J. Rudner, Activation of anti-oxidant Keap1/Nrf2 pathway modulates efficacy of dihydroartemisinin-based monotherapy and combinatory therapy with ionizing radiation, *Free Radic. Biol. Med.* 168 (2021) 44–54.
- [59] L. Yuan, S. Li, Q. Chen, T. Xia, D. Luo, L. Li, S. Liu, S. Guo, L. Liu, C. Du, G. Jia, X. Li, Z. Lu, Z. Yang, H. Liu, H. Mai, L. Tang, EBV infection-induced GPX4 promotes chemoresistance and tumor progression in nasopharyngeal carcinoma, *Cell Death Differ.* 29 (2022) 1513–1527.